C II* ABSORPTION IN DAMPED Lyα SYSTEMS. II. A NEW WINDOW ON THE STAR FORMATION HISTORY OF THE UNIVERSE

Arthur M. Wolfe[1] and Eric Gawiser[1,2]

Department of Physics and Center for Astrophysics and Space Sciences, University of California, San Diego,
9500 Gilman Drive, Code 0424, La Jolla, CA 92093; awolfe@ucsd.edu, egawiser@ucsd.edu

and

Jason X. Prochaska[1]

University of California Observatories, Lick Observatory, University of California, Santa Cruz, CA 95464;
xavier@ucolick.org

ABSTRACT

Starting from the star formation rate (SFR) per unit area, $\dot{\psi}_*$, determined for damped Lyα systems (DLAs) using the C II* method, we obtain the SFR per unit comoving volume, $\dot{\rho}_*(z)$, at $z \approx 3$. Pure warm neutral medium (WNM) solutions are ruled out since they generate more bolometric background radiation than observed, but the two-phase solutions dominated by the cold neutral medium (CNM) are consistent with the backgrounds. We find that $\dot{\rho}_*(z)$ for DLAs agrees with the $\dot{\rho}_*(z)$ for the Lyman break galaxies (LBGs). Although the mass of produced stars indicated by the SFRs is consistent with the current densities of known stellar populations, the mass of metals produced by $z = 2.5$ is 30 times larger than detected in absorption in DLAs. Of the three possible solutions to this " missing metals " problem, the most likely appears to be that star formation occurs in compact bulge regions. We search for evidence of feedback and find no correlations between $\dot{\psi}_*$ and $N(\text{H I})$, but possible correlations between $\dot{\psi}_*$ and low-ion velocity width and $\dot{\psi}_*$ and metal abundance. We show that (1) the correlation between cooling rate and dust-to-gas ratio is positive evidence for grain photoelectric heating, (2) the cosmic microwave background (CMB) does not significantly populate the C II excited fine-structure states, and (3) the ratio of C II* to resonance-line optical depths is a sensitive probe of the multiphase structure of the DLA gas. We address recent arguments that DLAs are comprised only of WNM gas and show them to be inconclusive. Despite the rough agreement between $\dot{\rho}_*(z)$ for DLAs and LBGs, current evidence indicates that these are distinct populations.

Subject headings: galaxies: evolution — quasars: absorption lines

1. INTRODUCTION

This is the second of two papers describing a new method for obtaining star formation rates (SFRs) in damped Lyα systems (DLAs). In Wolfe, Prochaska, & Gawiser (2003, hereafter Paper I) we showed how measurements of C II* $\lambda 1335.7$ absorption lines in DLAs allow one to infer the cooling rate per H atom of the neutral gas. Since we assume steady state conditions, this equals the heating rate per H atom, which we use to infer the SFR per unit area, $\dot{\psi}_*$. We do this by assuming gas in DLAs to be heated by the same mechanism responsible for heating the interstellar medium (ISM) in the Milky Way, the grain photoelectric effect (Bakes & Tielens 1994; Weingartner & Draine 2001). In that case the heating rate is proportional to the product of the dust-to-gas ratio, κ, the photoelectric heating efficiency, ϵ, and the mean intensity of far-ultraviolet (FUV) radiation, J_ν; the latter is proportional to $\dot{\psi}_*$ for sources in a plane-parallel layer. Specifically, in Paper I we modeled DLAs as uniform gaseous disks with radius R and scale height h, in which the sources of FUV radiation were uniformly distributed. We also showed how κ can be deduced from

the [Fe/Si] and [Si/H] abundance ratios [recall $[\text{X/Y}] \equiv \log_{10}(\text{X/Y}) - \log_{10}(\text{X/Y})_\odot$] for the following assumptions about grain composition: grains were either carbonaceous as in the Galaxy (the " Gal " model) or silicates as in the SMC (the " SMC " model). We inferred κ by assuming the number of depleted C or Si atoms per depleted Fe atom to be the same in DLAs as in the ISM. Furthermore, we considered depletion ratios ranging from a minimal " nucleosynthetic ceiling " in which the intrinsic ratio $[\text{Fe/Si}]_{\text{int}} = -0.2$ to a maximal depletion ratio $[\text{Fe/Si}]_{\text{int}} = 0.0$ (see Prochaska & Wolfe 2002, hereafter PW02).

In Paper I we solved the transfer equation for J_ν and then calculated the thermal equilibrium of gas subjected to cosmic-ray and X-ray heating in addition to grain photoelectric heating. The gas was assumed to cool in the usual way, i.e., by emission of fine-structure, metastable, and Lyα lines, as well as grain recombination radiation. We found that gas can reside in two thermally stable states: a cold neutral medium (CNM) and a warm neutral medium (WNM; see Wolfire et al. 1995, hereafter W95). Typically, the densities and temperatures of the CNM and WNM are 10 cm^{-3} and 150 K and 0.2 cm^{-3} and 8000 K, respectively. We further assumed the CNM and WNM to be in pressure equilibrium at pressure $P_{\text{eq}} = (P_{\text{min}} P_{\text{max}})^{1/2}$, where P_{min} and P_{max} are the minimum and maximum pressures of the pressure versus density curve. We considered a CNM model in which the line of sight to the background QSO encounters comparable column densities of gas in the CNM and the WNM. We also

considered a WNM model in which the line of sight encountered only WNM gas at pressure equal to P_{eq}. Combining the measured heating rates with those predicted at the thermally stable gas densities, n_{CNM} and n_{WNM}, we obtained unique values for $\dot{\psi}_*$ for each DLA: one value for the CNM solution and the other for the WNM solution. We then averaged $\dot{\psi}_*$, for two redshift bins centered at $z = 2.15$ and 3.70, to derive the average SFR per unit physical area, $\langle\dot{\psi}_*(z)\rangle$. The WNM models result in significantly higher SFRs than the CNM models since the measured [C II] 158 μm cooling rate per H atom, l_c, is a small fraction of the total cooling rate in the WNM, whereas l_c equals the total cooling rate in the CNM (see Paper I).

This paper starts by considering quantities with cosmological significance. Specifically, in § 2 we combine $\langle\dot{\psi}_*(z)\rangle$ with the incidence of DLAs per unit absorption distance interval, $d\mathcal{N}/dX$ (Bahcall & Peebles 1969), to derive the SFR per unit comoving volume, $\dot{\rho}_*(z)$. We then derive the bolometric background intensity, I_{EBL}, for all model combinations. We show that the WNM models produce more background radiation than observed in every case and, as a result, are ruled out. By contrast, the CNM models are consistent with the observed values of I_{EBL}. We compute a consensus model that is an average over all the CNM models. We show that the resulting $\dot{\rho}_*(z)$ are comparable to $\dot{\rho}_*(z)$ inferred for the Lyman break galaxies (LBGs; Steidel et al. 1999). In § 3 we consider implications of these results. We compute the mass of stars and the mass of metals produced by the star formation history, $\dot{\rho}_*(z)$, of the consensus model. While the mass of stars is consistent with masses of current stellar populations, the mass of metals produced by $z = 2.5$ is more than 30 times the mass of metals inferred for DLAs at the same redshift. We discuss possible solutions to this dilemma, including a "bulge" model in which star formation is confined to a compact region located at the center of the extensive region creating C II* absorption. We consider independent evidence for (1) star formation and (2) the deposition of stellar energy into the absorbing gas, i.e., feedback. At this point the reader not interested in the physics of interstellar gas can turn to the final section, § 6. Having discussed various implications of our models, we proceed to test their self-consistency in § 4, where three tests are carried out. First, we find a statistically significant correlation between the [C II] 158 μm cooling rate per atom, l_c, and κ, which is consistent with grain photoelectric heating in a CNM. Second, we show that the spontaneous energy emission rate, l_c, reflects the cooling rate of the gas instead of the excitation level caused by cosmic microwave background (CMB) radiation. Third, we examine the ratio of C II* to resonance-line optical depths to look for evidence of shifts in gas phase. In § 5 we discuss arguments made by other authors against the presence of CNM gas in DLAs. A careful reassessment of these arguments shows that they do no rule out the presence of CNM gas in DLAs. A summary and concluding remarks are given in § 6.

Unless stated otherwise, we adopt an Einstein–de Sitter cosmology in which $\Omega_M = 1$, $\Omega_\Lambda = 0$, and $h = 0.5$ to facilitate comparison with published results.

2. COSMOLOGICAL QUANTITIES

We now turn to quantities with cosmological significance. We compute the SFR per unit comoving volume, $\dot{\rho}_*$. The redshift dependence of $\dot{\rho}_*$ implies a star formation history throughout spacetime that gives rise to background radiation. We calculate the bolometric intensity of this background radiation for the CNM and WNM models and compare the results with observations. We then construct a consensus CNM model for $\dot{\rho}_*(z)$, which is consistent with measurements of the background radiation.

2.1. The SFR per Unit Comoving Volume

The SFR per unit comoving volume for DLAs is given by

$$\dot{\rho}_*(z) = \langle\dot{\psi}_*(z)\rangle An_{co}(z) , \quad (1)$$

where $\langle\dot{\psi}_*(z)\rangle$ is the average SFR per unit area at redshift z and A and n_{co} are the average physical cross-sectional area and comoving density of the DLAs, respectively. While neither A nor n_{co} has been determined from observations, their product is known from the incidence of DLAs per unit absorption distance interval, $d\mathcal{N}/dX$ (e.g., Storrie-Lombardi & Wolfe 2000). We find

$$\frac{d\mathcal{N}}{dX} = A_p n_{co}(X), \quad (2)$$

where A_p is the average projection of A on the plane of the sky and $X(z)$, the absorption distance (Bahcall & Peebles 1969), is given by

$$\frac{dX}{dz} = \left(cH_0^{-1}\right)\left\{\frac{(1+z)^2}{\left[(1+z)^2(1+\Omega_M z) - z(z+2)\Omega_\Lambda\right]^{1/2}}\right\} . \quad (3)$$

As a result,

$$\dot{\rho}_*(z) = \langle\dot{\psi}_*(z)\rangle\left(\frac{A}{A_p}\right)\frac{d\mathcal{N}}{dX} . \quad (4)$$

We computed $\dot{\rho}_*$ by assuming the DLAs to be plane-parallel layers, i.e., $A/A_p = 2$, and by choosing an Einstein–de Sitter cosmology ($\Omega_M = 1$, $\Omega_\Lambda = 0$, $h = 0.5$). Although this model is ruled out by observations (e.g., Bennett et al. 2003), it is the model used in most published determinations of $\dot{\rho}_*$ (e.g., Steidel et al. 1999; Lanzetta et al. 2002), and for this reason we selected it for purposes of comparison. We chose $\langle\dot{\psi}_*(z)\rangle$ and its associated errors from Table 3 in Paper I and calculated $d\mathcal{N}/dX$ at the mean z of the redshift bins from the expression

$$\frac{d\mathcal{N}}{dX} = \left(\frac{H_0}{c}\right)0.055(1+z)^{0.61} , \quad (5)$$

found by Storrie-Lombardi & Wolfe (2000) for the Einstein–de Sitter cosmology. Errors in $\dot{\rho}_*$ were computed by propagating errors in $\dot{\psi}_*$ and $d\mathcal{N}/dX$.

The results for the "Gal" dust models are shown in Figure 1 as magenta data points for minimal depletion and green data points for maximal depletion. As expected, the SFRs per unit comoving volume for the WNM models (Fig. 1b) are at least 10 times higher than for the corresponding CNM models (Fig. 1a). Furthermore, for every model, minimal depletion gives rise to higher $\dot{\rho}_*$ than the maximal depletion. This is because for a given heating rate, $\dot{\psi}_*$ is inversely proportional to the dust-to-gas ratio, κ, and κ is lower for minimal depletion than for maximal depletion. Figure 1 also reveals no evidence for statistically significant
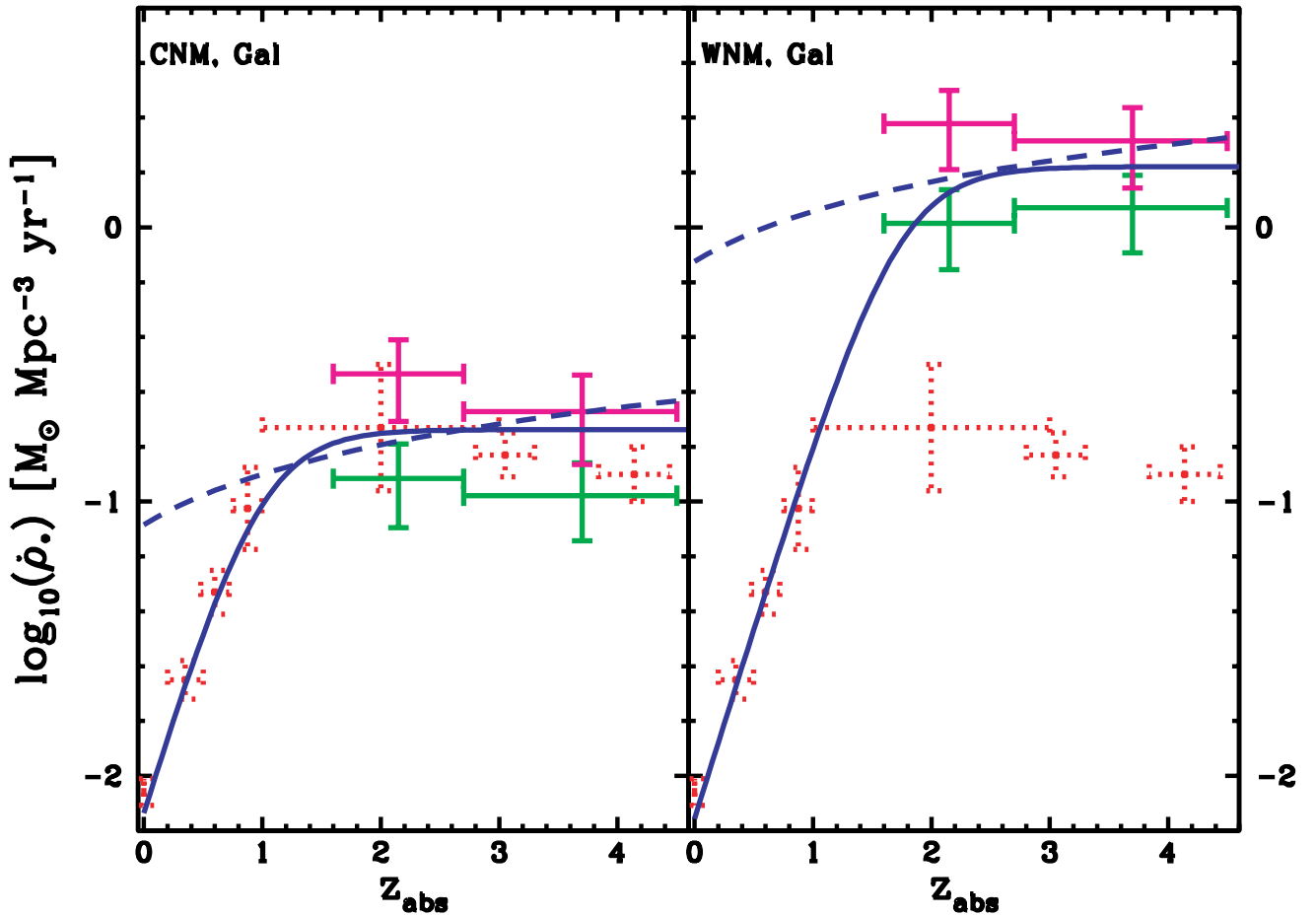
Fig. 1.—SFRs per unit comoving volume for "Gal" dust model shown as magenta data points for minimal depletion and green data points for maximal depletion. (a) Results for CNM model; (b) results for WNM model. Red dotted data points depict $\dot{\rho}_*$ inferred from galaxy luminosities (e.g., Steidel et al. 1999; Lilly et al. 1996; Barger et al. 2000). Solid blue curves are fits to high-z DLA data that also agree with galaxy data at $z < 1$. Dashed blue curves are fits to medians of DLA SFRs and are extrapolated to low z assuming that $\langle \dot{\psi}_*(z) \rangle$ is constant and combining eqs. (5) and (4).

redshift evolution of $\dot{\rho}_*$ determined by the C II* technique. This is in accord with determinations of $\dot{\rho}_*$ from luminosities measured for flux-limited samples of galaxies, shown as red data points. For the galaxy sample the SFRs in the two highest redshift bins are based on LBGs that are luminous at rest-frame UV wavelengths (Steidel et al. 1999), while the four lowest redshift points are based on galaxies with lower luminosities (Lilly et al. 1996). The bin at $z = 2$ is based on far-infrared (FIR) luminous galaxies detected by SCUBA (Holland et al. 1999). The redshifts for these objects were determined from a still uncertain radio-FIR photometric redshift indicator (Barger, Cowie, & Richards 2000). Interestingly, the magnitudes of the comoving SFRs deduced by the C II* and galaxy luminosity techniques are not very different in the redshift interval where they overlap, i.e., $z \approx [2, 4.5]$. For the CNM model the results are consistent within the errors, while for the WNM model the difference is about a factor of 10. We discuss possible implications of this agreement in §§ 2.3 and 6.

To test the generality of these conclusions, the calculations were repeated for the "SMC" dust models. The results, shown in Figure 2, reveal the same patterns as found for "Gal" dust. The principal difference is the systematically higher values of $\dot{\rho}_*$ predicted by corresponding "SMC" models. This is because the photoelectric heating

efficiency of silicate grains is lower than that of carbonaceous grains (see Fig. 15 in Weingartner & Draine 2001), and as a result higher SFRs are required to achieve a given heating rate in the case of silicate (i.e., "SMC") grains. Comparison between Figures 1 and 2 also reveals smaller differences between $\dot{\rho}_*$ derived for minimal and maximal depletion in the case of "SMC" dust than for "Gal" dust. The phenomenon is present in the CNM model but not the WNM model. In the case of maximal depletion, $[C/H]_{gas}$ is larger by 0.2 dex than for minimal depletion, but an increase in $[C/H]_{gas}$ causes a decrease in n_{CNM}, which can increase $\dot{\psi}_*$ significantly if n_{CNM} intersects the rising $l_{cr}(n)$ curves caused by the transition from WNM to CNM temperatures (see Fig. 5 in Paper I). In the case of "SMC" dust this effect compensates for the decrease in $\dot{\psi}_*$ caused by the increase in κ discussed above because the heating rate Γ_d increases more rapidly with density than for "Gal" dust (Weingartner & Draine 2001). Consequently, the net difference in $\dot{\psi}_*$, and hence $\dot{\rho}_*$, is smaller for "SMC" than for "Gal" dust.

2.2. Bolometric Background Intensity

While the *general* trends in the $(\dot{\rho}_*, z)$-plane appear to be insensitive to our choice of model assumptions, large systematic uncertainties in the comoving SFRs remain.
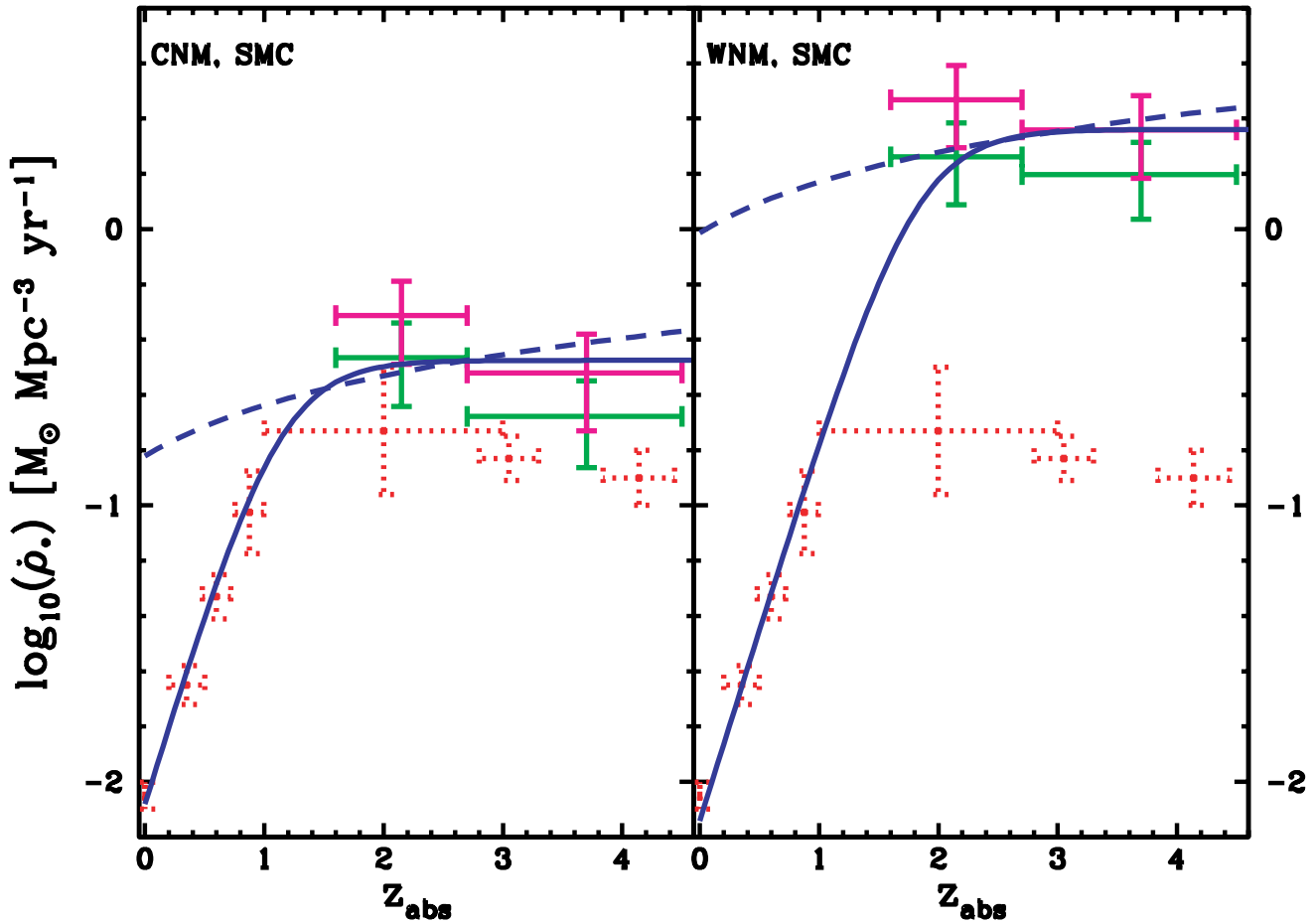
Fig. 2.—Same as Fig. 1, except "SMC" dust model is assumed

Although uncertainties in dust composition and depletion level are contributing factors, the largest source of error stems from uncertainties in the thermal phase. Does C II* absorption arise from gas in the CNM or WNM phase? To address this question, we compute the extragalactic bolometric background intensity, I_{EBL}. Because I_{EBL} is generated by a given star formation history, and since the star formation histories indicated by the CNM and WNM models are very different, measurements of the background intensity may be able to discriminate between them.

The bolometric extragalactic background intensity generated by a given star formation history, $\dot{\rho}_*(z)$, is as follows:

$$I_{EBL} = \frac{c}{4\pi} \int_{t_F}^{t_0} \frac{dt}{1 + z(t)} \int_0^t \dot{\rho}_*(t - t')L(t')dt' , \quad (6)$$

where $L(t')$ is the bolometric luminosity per unit mass as a function of age t' of a stellar population with a specified initial mass function (IMF; Madau & Pozzetti 2000), t_F is the formation epoch of the stellar population, and t_0 is the current age of the universe. We tested the models by computing backgrounds generated by analytic fits to the C II* comoving SFRs. The fits are shown as smooth curves in Figures 1 and 2, and the backgrounds they generate are shown as corresponding curves in Figure 3.

First, we explored the hypothesis that high-z DLAs evolve into normal low-z galaxies. Evolution into normal galaxies is consistent with the recent identification of DLAs

at $z < 1$ with the local galaxy population (Zwaan, Briggs, & Verheijen 2002; Turnshek, Rao, & Nestor 2002; Rosenberg & Schneider 2003). In that case the star formation histories are constrained to pass through the comoving SFRs measured for galaxies at $z < 1$ and for DLAs at higher redshifts. The results are shown as solid blue curves for "Gal" dust in Figure 1 and "SMC" dust in Figure 2. For the CNM model (Figs. 1a and 2a) the curves resemble the star formation histories inferred from galaxy luminosities in the redshift interval $z = [0, 5]$. For the WNM model (Figs. 1b and 2b) the fits greatly exceed the comoving SFRs inferred for the LBGs at $z > 2$, although they are in good agreement with the galaxy data at $z < 1$. Here the DLAs could represent a population of objects undetected in emission at high z that evolve into normal galaxies at low redshifts. Second, we considered a hypothesis in which the star formation histories of DLAs are dictated solely by their redshift evolution, without regard to the galaxy data. In this case we combined the expression for $\dot{\rho}_*(z)$ in equation (4) with the expression for $d\mathcal{N}/dX$ in equation (5). Although we find that $\langle \dot{\psi}_*(z) \rangle$ is independent of redshift in the redshift interval $z = [1.6, 4.5]$, at lower redshifts there are no measurements of C II*, and as a result $\langle \dot{\psi}_*(z) \rangle$ is unknown. Low redshifts are crucial because that is where most of the background radiation arises. For simplicity we let $\langle \dot{\psi}_*(z) \rangle$ equal a constant evaluated by averaging over all the $\dot{\psi}_*$ inferred from C II* absorption. The results are shown as dashed curves in Figures 1 and 2.
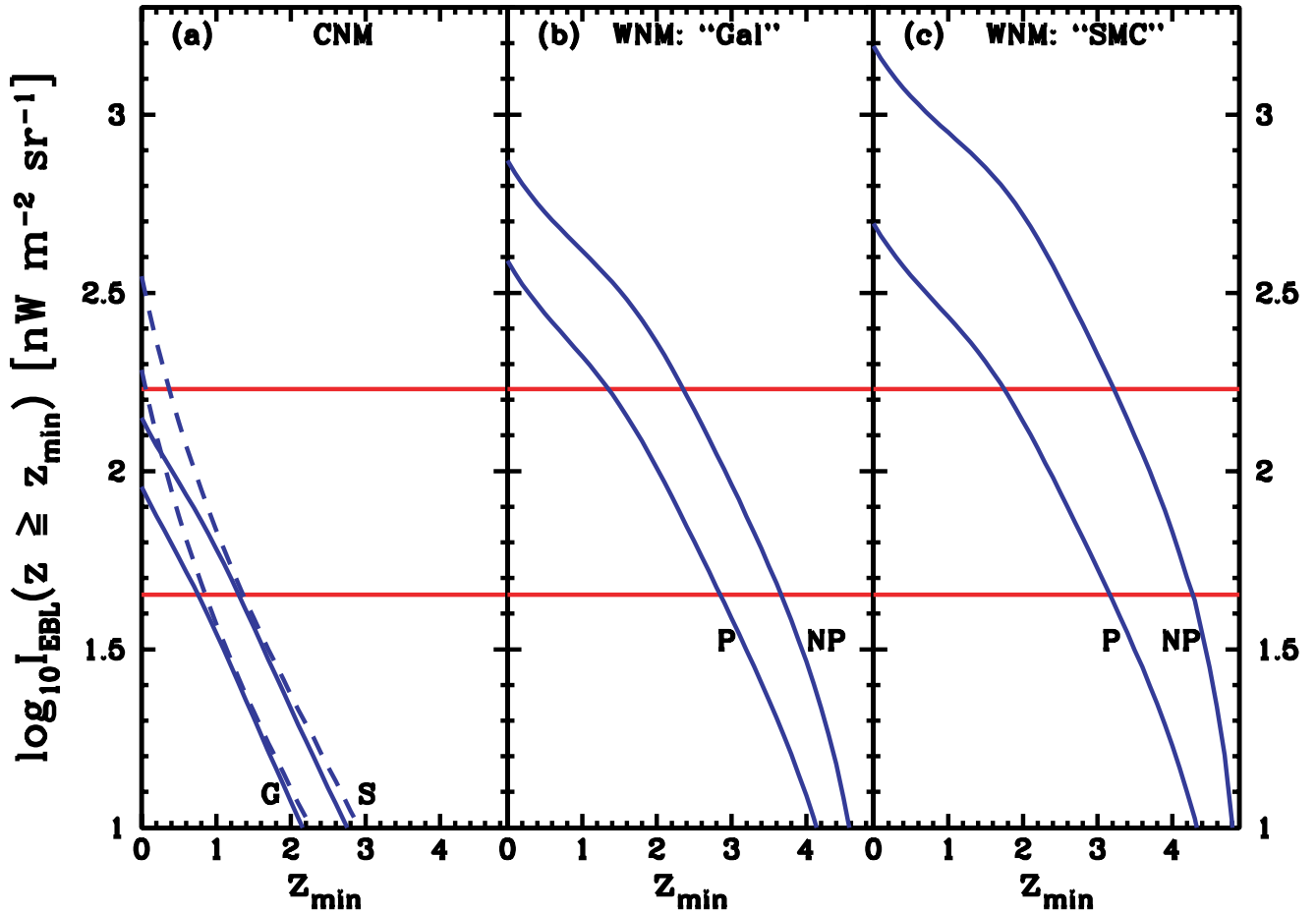
FIG. 3.—Smooth curves depict bolometric background intensity due to DLAs with $z \geq z_{min}$. Horizontal lines are empirical 95% confidence upper and lower limits. (a) Solutions for CNM model. Dashed curves labeled "G" and "S" are generated by "Gal" and "SMC" star formation histories shown as dashed curves in Figs. 1a and 2a. Solid curves so labeled are generated by "Gal" and "SMC" star formation histories shown as solid curves in Figs. 1a and 2a. (b) Solutions for WNM model for "Gal" dust. Curve labeled "P" is background generated by solid curve in Fig. 1b, in which optical pumping is included. Curve labeled "NP" is result without optical pumping. (c) Same as (b), except that the "SMC" star formation history of Fig. 2b is used.

The resulting backgrounds are shown in Figure 3, where we plot the predicted bolometric intensity from DLAs with $z \geq z_{min}$ versus z_{min}. The significance of this quantity, $I_{EBL}(z \geq z_{min})$, is that it reveals the contribution to the measured background, I_{EBL} [i.e., $I_{EBL}(z \geq 0)$], made by DLAs in the redshift range for which $\dot{\rho}_*(z)$ has been determined, i.e., $z = [1.6, 4.5]$. The backgrounds were obtained with an Einstein–de Sitter cosmology assuming $h = 0.5$, by adopting the same IMF used to relate $\dot{\psi}_*$ to mean intensity (see Paper I), using Bruzual & Charlot's (1993) population synthesis libraries (see Madau & Pozzetti 2000), and assuming a formation redshift $z_F = 5$. For comparison, the two horizontal straight lines depict upper and lower limits on I_{EBL} set by measurements between 0.15 and 1000 μm (Hauser & Dwek 2001). This wavelength range is relevant since it brackets the background spectra predicted for most models of DLAs (e.g., Pei, Fall, & Hauser 1999). According to E. Dwek (2002, private communication), the upper limits, which are crucial here, are conservative and should be regarded as 95% confidence limits. It is important to emphasize that while $\dot{\rho}_*(z)$ is cosmology dependent, the backgrounds computed from the C II* technique (i.e., by combining eqs. [4] and [6]) are independent of the adopted cosmology and Hubble constant. Therefore, consistency

between theory and observation is independent of the cosmology one assumes.

The background intensities predicted for the WNM models are too high. Figures 3b and 3c depict backgrounds generated by the "Gal" and "SMC" dust models, respectively. The curves labeled "P" correspond to the star formation histories generated by the solid curves in Figures 1b and 2b, where "P" indicates that optical pumping is included (where optical pumping is the mechanism by which the populations of the ground-term fine-structure states are mixed through UV excitations to higher lying levels; e.g., Sarazin, Rybicki, & Flannery 1979). The curves labeled "NP" show backgrounds generated by star formation histories without optical pumping. As discussed in Paper I, the true WNM solution lies between these limits. The predicted background for the "Gal" model is between 2.5 and 5 times the 95% confidence upper limit on I_{EBL}, and between 3 and 10 times this limit for the "SMC" model. In both models, sources with $z \geq z_{min} = 1.6$ generate background intensities exceeding the 95% confidence upper limit, indicating that DLAs in which C II* absorption arises in WNM gas produce more background radiation than observed. When the contribution of lower z galaxies is included, the observed upper limits to the backgrounds are exceeded by much

larger factors. Had we computed backgrounds generated by the dashed curves in Figures 1b and 2b, we would reach the same conclusion, i.e., the WNM models are ruled out.

This disproof of the WNM-dominated solution appears to be robust. The FUV mean intensities inferred for four DLAs in which H_2 is detected (Ge & Bechtold 1997; Srianand, Petitjean, & Ledoux 2000; Molaro et al. 2002; Levshakov et al. 2002) are comparable to $G_0 = 1.7$, the value found for the Galaxy ISM (Draine 1978; note that G_0 is J_ν in convenient units of 10^{-19} ergs cm^{-2} s^{-1} Hz^{-1} sr^{-1}). Although these results may need to be corrected for suppression of optical pumping (Sarazin et al. 1979), the implication is that $\langle \dot{\psi}_* \rangle$ is significantly lower than required by the WNM models. Furthermore, the backgrounds predicted for the WNM models are conservative lower limits. This is because we assumed the pressure of the two-phase medium, P_{eq}, to exceed P_{min}, the maximum pressure allowed for gas in a pure WNM phase. Values of $P_{eq} < P_{min}$ would result in lower values of n_{WNM} and hence higher $\dot{\rho}_*$. Note that high values of $\dot{\rho}_*$ are predicted even if C II* absorption arises in warm gas with temperatures below that predicted by our two-phase model. We considered scenarios in which C II* absorption arises in gas with $T \sim 1000$ K, i.e., in thermally unstable gas like that predicted by Vazquez-Semadeni, Gazol, & Scalo (2000). Figure 3c in Paper I shows that at such temperatures the total cooling rate is considerably larger than the 158 μm emission rate, especially in the absence of optical pumping. The resulting backgrounds are significantly above the 95% confidence upper limit on I_{EBL} when the emission from $z < 1$ galaxies is added to the contribution from DLAs. Therefore, WNM models, or any model in which [C II] 158 μm emission does not dominate the cooling rate, are unlikely to be correct.

By contrast, CNM models in which $\langle \dot{\psi}_*(z) \rangle$ decreases with decreasing redshift are consistent with the background data. Consider models in which $\langle \dot{\psi}_* \rangle$ equals a constant given by the average of all the inferred values of $\dot{\psi}_*$ for the CNM models. These are depicted by dashed curves in Figure 3a and correspond to the "Gal" (G) and "SMC" (S) star formation histories shown as dashed curves in Figures 1a and 2a. Both models predict $I_{EBL}(z \geq 0)$ to be above the 95% confidence upper limit on bolometric intensity. Moreover, Figures 1a and 2a show that $\dot{\rho}_*$ at $z = 0$ is significantly above the comoving SFR inferred from the luminosities of local galaxies. On the other hand, the solid curves in Figures 1a and 2a depict model star formation histories that are compatible with $\dot{\rho}_*(z)$ inferred for galaxies at $z < 1$. These curves generate the backgrounds shown as solid curves in Figure 3a, which are compatible with the limits on I_{EBL}. For these models $\langle \dot{\psi}_*(z) \rangle$ at $z = 0$ must be significantly below the $\approx 10^{-2.2}$ $M_\odot$ yr^{-1} kpc^{-2} determined at high redshifts for both "Gal" and "SMC" dust. At first, this appears to be inconsistent with the observation that $\langle \dot{\psi}_* \rangle$ deduced for local disk galaxies is comparable to $10^{-2.4}$ $M_\odot$ yr^{-1} kpc^{-2} (Kennicutt 1998). However, the latter star formation estimates were made by averaging over the corrected de Vaucouleurs radius, R_0, whereas DLA absorption at any redshift would occur out to an average radius $R_{H I} \approx 2R_0$ (Wolfe et al. 1986). However, to compute $\dot{\rho}_*$, it is necessary to average $\dot{\psi}_*$ over $R_{H I}$, not R_0. Therefore, the appropriate value of $\langle \dot{\psi}_* \rangle$ for local disk galaxies should be reduced by a factor of 4 to $10^{-3.0}$ $M_\odot$ yr^{-1} kpc^{-2}. We conclude that if DLAs evolve into normal galaxies, their SFR per unit area has decreased significantly since $z \approx 1.6$. We emphasize that

this conclusion holds for $\dot{\psi}_*$ averaged over $R_{H I}$ rather than R_0, which is normally used for computing $\dot{\psi}_*$ in nearby galaxies (Kennicutt 1998).[3]

2.3. *Consensus Star Formation Model*

By ruling out the WNM hypothesis, we have eliminated half the models discussed so far. Nevertheless, the remaining CNM models contain significant systematic uncertainties, as indicated by the scatter among $\dot{\rho}_*(z)$ inferred from the various dust hypotheses (Figs. 1a and 2a). Here we attempt to assess these errors, as well as errors due to other effects, and to deduce consensus values for $\dot{\rho}_*(z)$.

To estimate the size of the systematic errors, we test the sensitivity of the CNM models to variations of crucial input parameters. We find $\dot{\rho}_*(z)$ to be sensitive to changes in equilibrium pressure, P_{eq}, and that the effect is similar in magnitude to the scatter in $\dot{\rho}_*(z)$ due to uncertainties in the composition and depletion level of dust. The results in Figures 1 and 2 were computed assuming $P_{eq} = (P_{min}P_{max})^{1/2}$. Because of the uncertainties surrounding this criterion (see discussion in Paper I), we now consider the effects of letting P_{eq} vary between P_{min} and P_{max}. We find that $\dot{\rho}_*$ decreases with increasing P_{eq}. As P_{eq} rises, n_{CNM} increases, which results in lower values of $\dot{\psi}_*$ for a fixed l_c (see Fig. 5 in Paper I). Therefore, $\dot{\rho}_*$ is a minimum when $P_{eq} = P_{max}$ and a maximum when $P_{eq} = P_{min}$. We assume that the variances in $\dot{\rho}_*$ are determined by differences between these limiting values of $\dot{\rho}_*$ and the means defined by $P_{eq} = (P_{min}P_{max})^{1/2}$. It is possible to increase the variances in $\dot{\rho}_*$ further by reducing the standard ratio of cosmic-ray ionization rate, ζ_{CR}, to the SFR per unit area, $\dot{\psi}_*$, given in equation (9) in Paper I. However, the consequent increase in $\dot{\rho}_*$ is constrained by the upper limit on I_{EBL} to $\log_{10} \dot{\rho}_* < -0.2$ $M_\odot$ yr^{-1} Mpc^{-3}, while the decrease is limited to $\log_{10} \dot{\rho}_* > -1.5$ $M_\odot$ yr^{-1} Mpc^{-3} by the observed ratios of C II to C I column densities, which become too small when $\zeta_{CR}/\dot{\psi}_*$ is more than twice the standard value (see § 5.1). Although it is possible for $\dot{\rho}_*$ to attain these extreme values, it is more likely to remain within the standard limits, which justifies their use in constructing the variances. Similar procedures were used to compute variances in $\dot{\rho}_*$ due to variations in other input parameters such as the ratio of the radius to height, R/h, of the model uniform disk (see Fig. 4 in Paper I).

In order to compute consensus values of $\dot{\rho}_*(z)$ in a given redshift bin, we considered all four possible combinations of "Gal" versus "SMC" dust composition and minimal versus maximal depletion. For each of these four models we determined the probability distribution of $\dot{\rho}_*(z)$ using the best-fit value and an error budget that included (1) varying P_{eq} from P_{min} to P_{max}, (2) varying the aspect ratio R/h between minimum and maximum values, and (3) the random errors appearing in Figures 1 and 2. Although we

---

[3] When we compared the average l_c in DLAs to the average l_c for the ISM (Paper I), we found that the ratio $(l_c)_{DLA}/(l_c)_{ISM}$ roughly equaled the average dust-to-gas ratio of DLAs relative to that of the ISM, i.e., κ. This indicated that G_0 in DLAs is roughly equal to the ISM value, $G_0 = 1.7$, which corresponds to $\dot{\psi}_* = 10^{-2.4}$ $M_\odot$ yr^{-1} kpc^{-2}. Does this contradict our finding that $\dot{\psi}_*$ at $z = 0$ equals $10^{-3.0}$ $M_\odot$ yr^{-1} kpc^{-2}? The answer is no because the high opacity of dust in the ISM indicates that G_0 arises mainly from local sources within the optical radius, whereas the lower opacity of dust in DLAs indicates that G_0 inferred from C II* absorption lines is a global average, which includes the very low SFRs occurring outside the optical radius.

suspect that "SMC" dust and minimal depletion are more likely to be correct, we conservatively assumed that all four models were equally likely. We performed a Monte Carlo simulation drawing an equal number of simulated data points from each of the four model probability distributions. Note that this is equivalent to a Monte Carlo simulation where each DLA is analyzed using all four models and then these $4n_{DLA}$ data points are resampled at random to generate the maximum possible variance. The resulting probability distribution for $\dot{\rho}_*(z)$ is well described by a Gaussian, and we computed the resulting mean, 68% confidence intervals, and 95% confidence intervals. There are additional systematic uncertainties that we are unable to quantify at present, including those due to uncertainties in the grain size distribution and others that we are unable to compute, such as possible radial variations in $\dot{\psi}_*$. We do not expect these additional sources of error to dominate. In particular, we show in § 3.2 that the error due to our assumption of spatially uniform $\dot{\psi}_*$ is probably less than 0.1 dex. The largest systematic uncertainty at present is produced primarily by the model with "Gal" dust composition and maximal depletion, so falsifying either the "Gal" or maximal depletion solutions would raise the result for $\dot{\rho}_*(z)$ and significantly reduce the uncertainty.

The consensus "Madau" diagram for DLAs is shown in Figure 4. The results are for the Einstein–de Sitter cosmology, and the interested reader is referred to Table 1, where

we compare these with $\dot{\rho}_*$ inferred for the standard Λ cosmology; the differences are of order 0.1 dex. The error bars (corresponding to 68% confidence levels) are of course larger than in Figures 1 and 2, which include only random errors. Although our errors are larger than reported for the LBGs, the latter errors do *not* include systematic errors such as extinction corrections to galaxy luminosities, which are surely present (see discussion in Steidel et al. 1999). By contrast, the effects of dust are essential features of our models. Moreover, the low values of κ imply that at least half of the radiation from the disk is emitted at rest-frame FUV wavelengths; i.e., our dust correction is less than a factor of 2. The blue curve is our eyeball fit through the DLA and low-z
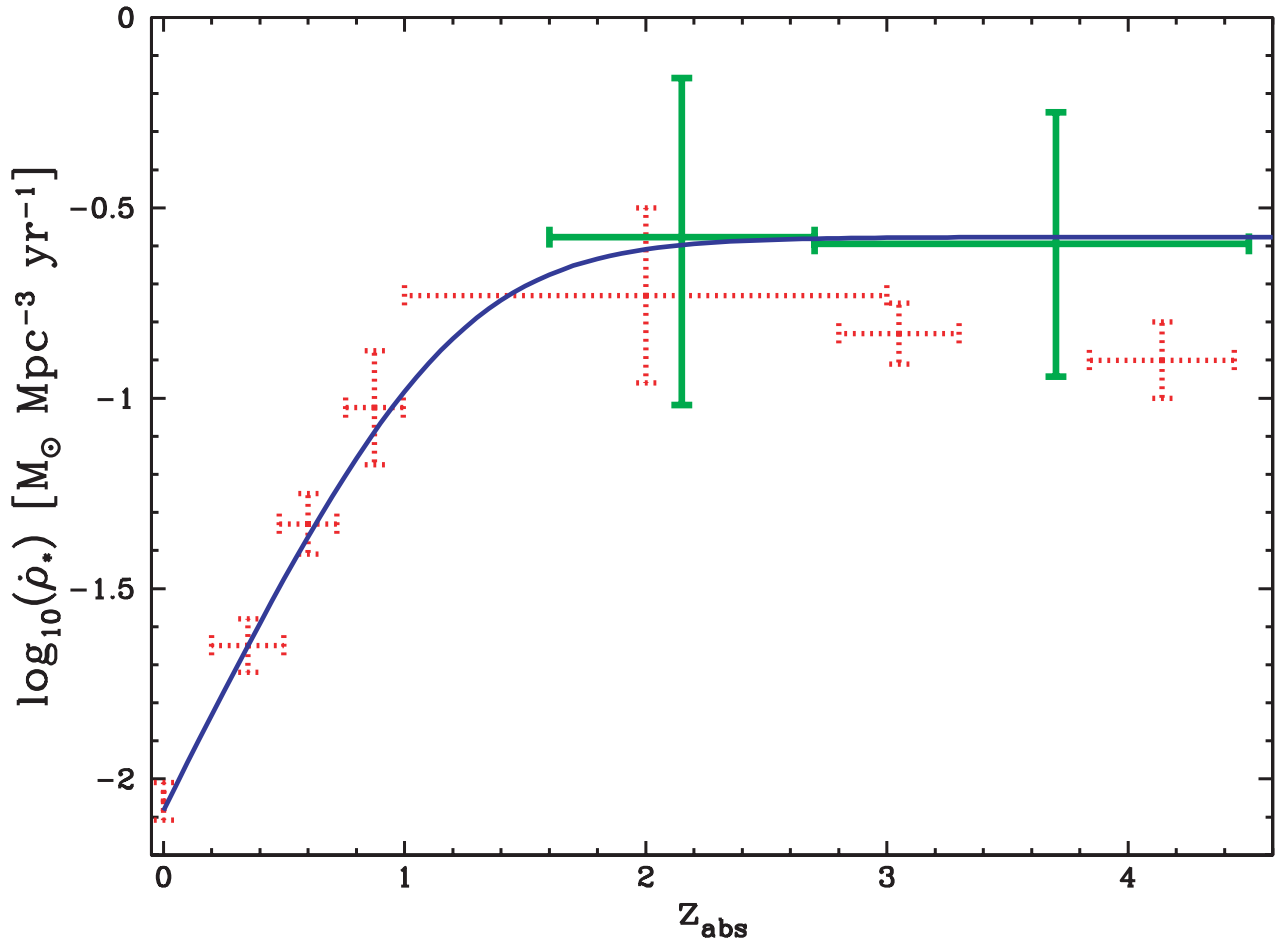
TABLE 1
COSMOLOGY DEPENDENCE OF $\dot{\rho}_*$ FOR
CONSENSUS MODEL

| | $\log_{10} \dot{\rho}_*$ | |
| | $(M_\odot \, yr^{-1} \, Mpc^{-3})$ | |
z	Einstein–de Sitter[a]	Standard Λ[b]
2.15	-0.58 ± 0.42	-0.68 ± 0.42
3.70	-0.59 ± 0.35	-0.71 ± 0.35

[a] Cosmology with $\Omega_M = 1, \Omega_\Lambda = 0, h = 0.5$.
[b] Cosmology with $\Omega_M = 0.3, \Omega_\Lambda = 0.7, h = 0.7$.

FIG. 4.—Green data points depict $\dot{\rho}_*$ and 68% confidence errors for "consensus" model described in § 2.3. Dotted data points are galaxy data described in previous figures. Smooth curve is eyeball fit to "consensus" model at high z and galaxy data at low z.

galaxy data in this diagram and will be used in the following section to compute integrated quantities such as the mass in stars and metals produced over various timescales. Of course, it is possible that high-z DLAs do *not* evolve into low-z DLAs and their associated galaxies but instead evolve into a population of objects with luminosity density far below that of normal galaxies. While we cannot rule out this scenario altogether, we believe it is implausible. The principal argument against it is the agreement between the comoving mass density of neutral gas in high-z DLAs and the mass density of visible matter in current galaxies (Storrie-Lombardi & Wolfe 2000). This indicates a connection between DLAs at high redshift and those at low redshift, unless one assumes that this agreement is a random coincidence. As a result, the most likely scenario is one in which $\langle \dot{\psi}_*(z) \rangle$ decreases in time at $z < 1.6$ in such a way that the DLAs evolve into low-z galaxies.

Figure 4 also shows consistency with $\dot{\rho}_*(z)$ inferred from gas consumption in DLAs (Pei et al. 1999), which lends credibility to the idea that the decline with time of the comoving density of neutral gas is related to star formation. Furthermore, Figure 4 indicates approximate agreement between $\dot{\rho}_*(z)$ determined for DLAs and LBGs. That measurements of the same quantity by independent techniques based on different physical considerations are even in approximate agreement either is a coincidence or indicates a connection between DLAs and LBGs. We shall address this issue in § 6.

3. IMPLICATIONS

In this section we discuss several consequences of this work. In particular, we discuss (1) the production of stars and metals implied by the derived $\dot{\rho}_*(z)$, (2) a scenario in which star formation is confined to a centrally located bulge, and (3) evidence for feedback.

3.1. *Baryon and Metal Production*

Having determined $\dot{\rho}_*(z)$ for DLAs, we can integrate under the smooth curve in Figure 4 to obtain $\rho_*(z)$, the comoving mass density of stars at redshift z. We find

$$\rho_*(z) = \int_z^{z_F} \dot{\rho}_* \left| \frac{dt}{dz} \right| dz , \qquad (7)$$

where this expression for $\rho_*(z)$ is independent of cosmology and Hubble constant when $\dot{\rho}_*(z)$ is determined from the C II* technique, i.e., from equation (4). Note that unlike I_{EBL}, this integral receives considerable weight from $z > 1.6$. Pettini (1999) used the last equation to determine $\rho_*(0)$, the current mass density in stars formed by the LBGs. Our estimate of $\rho_*(0)$ for DLAs, which we obtain by integrating the last equation from $z = 0$ to z_F, is shown in Figure 5 along with 68% confidence intervals. We compare this to determinations of the current mass densities of stars formed by LBGs and other stellar populations (Fukugita, Hogan, & Peebles 1998). In deriving this result we (1) integrated to the present under the solid curve shown in the figure and (2) multiplied by Leitherer's (1998) correction factor of 0.4 (adopted to correct for a more realistic IMF; see Pettini 1999). Figure 5 shows that DLAs and LBGs produce the same mass in stars to within 1 σ. Moreover, the star formation history of DLAs suffices to produce the observed stellar content of spheroids, bulges of spirals, and spiral disks.
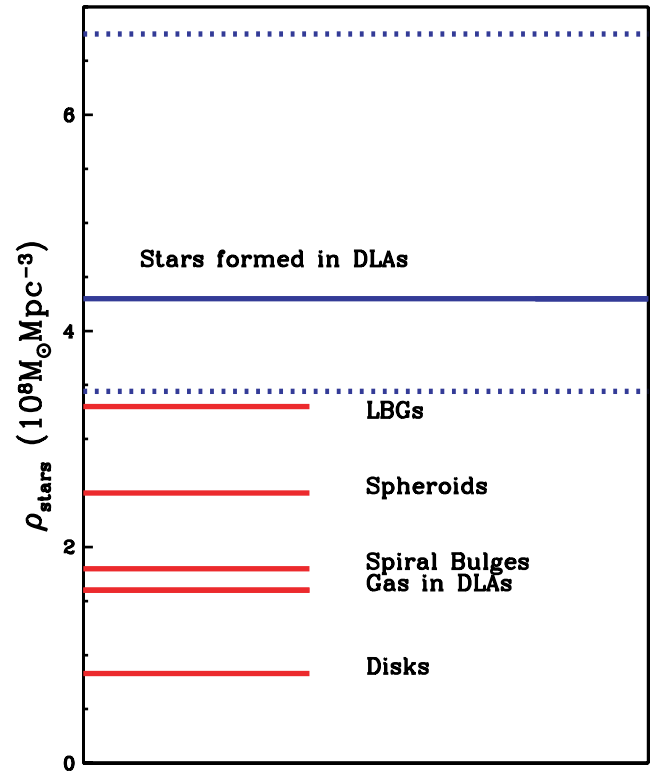

FIG. 5.—Mass density of stars per unit comoving volume for various populations. The solid blue horizontal line depicts density produced by SFR for DLAs. Dotted blue lines are 68% confidence level error bars. Red horizontal lines depict corresponding densities for stars formed by LBGs, current spheroids, current spiral bulges, and current spiral disks. "Gas in DLAs" corresponds to comoving mass density of gas in DLAs at $z \approx 3$.

Although the indicated uncertainties in $\rho_*(0)$ are large, the similarity between the predicted stellar content of DLAs and observed stellar content of galaxies is consistent with the idea that their progenitors were DLAs (e.g., Wolfe 1995). In addition, the similarity between the comoving gas density in DLAs at $z \sim 3$ (Storrie-Lombardi & Wolfe 2000) and $\rho_*(0)$ is further evidence of self-consistency, although some infall might be required if the gas density is really lower than $\rho_*(0)$.

We also updated Pettini's (1999) calculation for the mass of metals produced by $z = 2.5$, the median redshift of DLAs for which metal abundances have been determined (Pettini et al. 1994; PW02). Pettini (1999) obtained this result using comoving SFRs for LBGs, whereas we use comoving SFRs for DLAs. The result shown in Figure 6 was computed assuming $\dot{\rho}_{metals} = (1/42)\dot{\rho}_*$ (Madau et al. 1996) and is compared with the comoving density of metals in $z = 2.5$ DLAs and with the current mass density of metals in spiral bulges.

Clearly the metals produced are sufficient to account for the metal content of spiral bulges. However, as discussed by Pettini (1999), the mass density of produced metals is 30 times higher than metals observed in DLAs. The difference is significant, since, as shown in Figure 6, the observed metal content of DLAs is well below the 95% confidence contour predicted for the produced metal content. Therefore, the difference between observed and produced metal content is real and leads to a "missing metals" problem. Pettini (1999) first noticed this problem when he found that the metals produced in LBGs exceeded the metals measured in
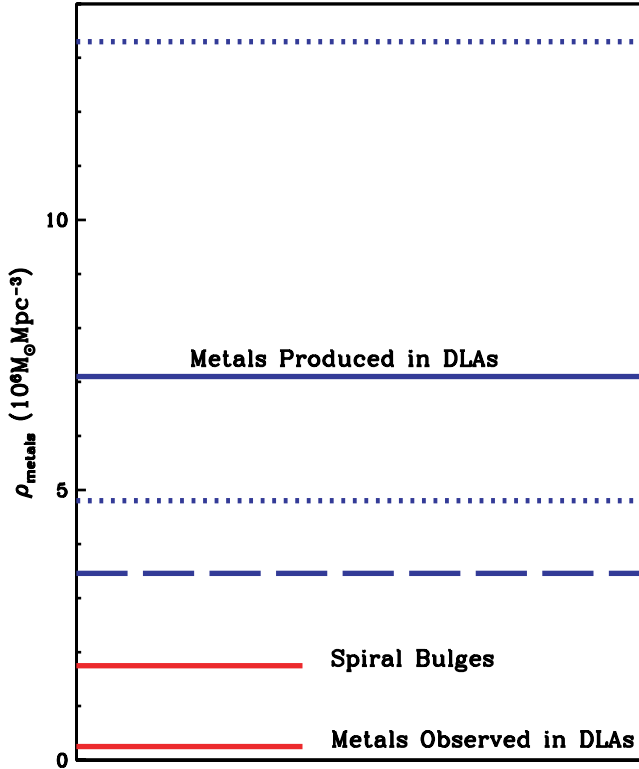
FIG. 6.—Comoving mass density of metals. The solid blue line shows metals produced in DLAs by $z = 2.5$. Dotted blue lines are corresponding 68% confidence contours, and the dashed blue line is the lower 95% contour. Red lines correspond to density of metals in spiral bulges and in DLAs.

DLAs. The problem is much more severe in our case because we are measuring both metal production and metal content in the *same population*.

Three possible solutions to the missing metals problem are to sequester the metals produced away from the DLA gas observed at $z \sim 2.5$, by confining these metals either in "bulges," in different systems, or in the IGM. The first solution requires that most of the star formation we are seeing is occurring in a compact region, i.e., a bulge, and metals produced in this region do not rapidly enrich the rest of the gas of the galaxy beyond the low metallicities observed in DLAs. The second solution requires that DLAs are a transitory phase early in the formation of galaxies, meaning that by the time significant metals have been produced the neutral gas has already been used up. Hence, the objects observed as DLAs at $z \sim 2.5$ are entirely distinct from objects that follow the DLA star formation history starting at formation redshifts $z > 4$. The third solution is to allow the metal-enriched material of supernovae to blow out of the DLA galaxy (Mac Low & Ferrara 1999). We see two problems with blowout. First, the efficiency of ejecting metal-enriched gas must exceed $1 - (29/30) = 0.97$, which is much larger than the maximum efficiency of 0.5 seen in local starburst galaxies (C. Martin 2003, private communication). Second, such ejection would result in a mean IGM metallicity, $[M/H] = -1.2$, which is at least 2 orders of magnitude larger than the metallicity of the Lyα forest (Songaila 2001); this would require placing most of the metals in the high-z IGM in some undetectable state. In the next subsection we shall explore the solution we find most appealing,

the bulge hypothesis. Other possible explanations include changing the IMF from that assumed by Pettini (1999) (which is the same Madau et al. 1996 IMF used in our previous computations) so that lower masses of metals are released at the endpoints of stellar evolution.

3.2. *Bulge Hypothesis*

Suppose star formation is concentrated in the central regions of DLAs, e.g., in protobulges, which at early times could be configurations of molecular clouds that are rarely detected in DLAs because of a small covering factor or possible obscuration by dust. In that case most of the metals would be released in the bulge, which would explain why the mass of metals produced in DLAs is consistent with the mass of metals in spiral bulges within the errors, as shown in Figure 6. The Milky Way bulge is relevant since it is a metal-rich but old population of stars, most of which formed by $z = 2.5$ (Wyse, Gilmore, & Franx 1997). In this picture a small fraction of the metals produced would find their way to the outer disk via stellar winds or supernova explosions, thereby explaining the lower metallicities of the DLA gas. This idea is self-consistent since, as we now show, the higher SFR per unit area in the central region can account for the heating rates inferred from the C II* observations of the outer disk without significantly increasing $\dot{\rho}_*$.

For simplicity, let the bulge be a sphere with radius R_B, which is located at the center of a uniform disk with radius R and half-thickness h. In this scenario the disk gives rise to damped Lyα and C II* absorption, while FUV radiation *emitted* by the bulge is the source of the mean intensity at radius r, $J_\nu^B(r)$, which heats the gas through grain photoelectric emission. In that case the mean intensity is given by

$$J_\nu^B(r) = \frac{L_\nu}{(4\pi)^2 r^2} \exp(-k_\nu r) , \qquad (8)$$

where $R_B < r < R$, L_ν is the luminosity per unit frequency bandwidth of FUV starlight emitted by the bulge, and k_ν is the absorption opacity due to dust in the uniform disk.

The radiation intensity inferred from DLAs by our method represents an average over all possible lines of sight through these uniform disks, where the C II* column determined for each system represents the average of all gas along that particular line of sight. We approximate this "average of averages" as a simple average of the radiation intensity received at all points in the disk, i.e.,

$$\langle J_\nu^B \rangle = \frac{2}{\pi R^2 2h(4\pi)}$$
$$\times \int_0^{2\pi} d\phi \left(\int_0^{\theta_c} \int_{R_B}^{h \sec \theta} r^2 \sin \theta \, d\theta \, dr \, L_\nu \frac{e^{-k_\nu r}}{4\pi r^2} \right.$$
$$\left. + \int_{\theta_c}^{\pi/2} \int_{R_B}^{R \csc \theta} r^2 \sin \theta \, d\theta \, dr \, L_\nu \frac{e^{-k_\nu r}}{4\pi r^2} \right) , \qquad (9)$$

where we have assumed $R_B < h$, which seems reasonable for the thick disks expected at high redshift. Except for the R_B limit, this expression is equivalent to the solution for J_ν obtained for uniform disks (eq. [14] in Paper I) since the luminosity density of such disks is $\rho_\nu = L_\nu/(\pi R^2 2h)$. This occurs because of the symmetry between the flux received at the center of a uniform disk from all points within the disk and the average flux received over a uniform disk from a

bulge located at its center. When integrated the solution looks just like that of equation (15) in Paper I except that the 1 is replaced by $\exp(-k_\nu R_B)$, which will be very close to 1 given that the entire disk is nearly optically thin (the bulge, of course, is likely to be optically thick and have a different value of k_ν, but our observations are sensitive to the FUV photons that successfully escape from the bulge region, so this does not affect the results). If $L_\nu/(\pi R^2 2h)$ is the same for the bulge and disk models, the expected values of radiation intensity are equal to an accuracy within 10%, i.e., $\langle J_\nu^B \rangle \simeq J_\nu^D$, where J_ν^D is the mean intensity computed for disks with a uniform distribution of sources in equation (14) in Paper I. Since these two models represent extremes of the source distribution (uniform vs. central source), we expect any intermediate source distributions to lead to similar values of radiation intensity. This is important since hierarchical structure formation implies that a given DLA could receive radiation from several compact regions of active star formation rather than a single central bulge. Because the SFRs per unit comoving volume for bulges or disks are given by

$$\dot{\rho}_* \propto L_\nu n_{co} , \tag{10}$$

the bulge-to-disk ratio $(\dot{\rho}_*)_B/(\dot{\rho}_*)_D = L_\nu^B/L_\nu^D$. Comparison between equation (14) in Paper I and equation (9) in this paper shows that this ratio equals the product of $\langle J_\nu^B \rangle / J_\nu^D$ and the ratio of the dimensionless integrals in both equations. To compare bulge and disk SFRs, we assume that $J_\nu^D = \langle J_\nu^B \rangle$ so that both models generate the observed heating rate. Because the dimensionless integrals are identical to within 10%, we find that $(\dot{\rho}_*)_B \approx (\dot{\rho}_*)_D$.

As a result, the estimates of $\dot{\rho}_*$ deduced for star formation throughout uniform disks do not change significantly when star formation is confined to the centers of such disks. Therefore, our estimates of $\dot{\rho}_*$ for disks do not appear to be very sensitive to the radial distribution of the sources of FUV radiation provided that the disks are optically thin to such radiation. Although the disks are likely to be optically thin, we cannot rule out the presence of optically thick dust in the bulge, which attenuates some fraction of the FUV radiation emitted by the stars. In that case the expression for $(\dot{\rho}_*)_B$ found by equating $\dot{\rho}_*$ for the disk and bulge models would be a lower limit to the actual SFR per unit comoving volume. Since we can increase $\dot{\rho}_*(z \geq 1.6)$ inferred for the consensus model, i.e., inferred from FUV heating, by a factor of 3.3 before the background is violated, the radiation attenuated in the bulge model can be as much as a factor of 2.3 times that observed; i.e., as much as 0.7 of the total FUV radiation can be attenuated.

We can also use the bulge model to compute the *total* SFRs, $\dot{M}_*$, required to explain the observed C II* heating rates. From equation (8) we find that $\dot{M}_* = 1.9(r/10 \text{ kpc})^2 G_0 \ M_\odot \text{ yr}^{-1}$, where we used the Madau et al. (1996) calibration to convert L_ν to $\dot{M}_*$. Assuming $G_0 = 6.8$, the average of the positive detections for the "Gal" minimal depletion model, we have $\dot{M}_* = 13(r/10 \text{ kpc})^2 \ M_\odot$ yr^{-1}. If we let r equal 10 kpc, a typical impact parameter, we find that $\dot{M}_*$ is consistent with upper limits obtained from Hα imaging of seven DLAs by Bunker et al. (2001). On the other hand, this SFR is about 3 times higher than the more sensitive NICMOS upper limits reported by Kulkarni et al. (2001) for the DLA toward Q1244+34. Unfortunately, we do not have C II* λ1335.7 profiles of this DLA. Future

searches for emission from DLAs with detected C II* absorption may prove to be sensitive tests of the bulge hypothesis. These tests will be less sensitive for the uniform disk models, where the predicted surface brightnesses are low. In any case the limits on $\dot{M}_*$ for the bulge hypothesis place severe constraints on rotating disk models in which $r \geq 20$ kpc is required (Prochaska & Wolfe 1997, hereafter PW97), since $\dot{M}_*$ for the central bulge will be higher than observational constraints allow.

3.3. *Search for Evidence of Star Formation and Feedback*

Stars leave imprints on the gas from which they form, and this may be detectable in DLAs. In the uniform disk scenario a correlation should exist between $\dot{\psi}_*$ and N(H I) resembling the Kennicutt relation found in nearby disk galaxies (Kennicutt 1998). This is a manifestation of the condensation of gas into stars, since it is equivalent to the Jeans instability criterion in rotating disks (Toomre 1964). Stars also deposit energy and other by-products of stellar evolution into the gas, and so one might expect to find evidence of feedback if the uniform disk scenario is correct. This would occur through shocks generated by supernova explosions. Because of the short main-sequence lifetimes of the progenitor stars, feedback is directly related to the SFR. By contrast, the connection between stars and DLA gas may not exist, or may be indirect, in the bulge scenario.

We test these ideas with SFRs derived from the CNM model with "Gal" dust and minimal depletion. The results of this investigation are statistically indistinguishable from those of "Gal" dust with maximal depletion and "SMC" dust with maximal or minimal depletion. The test of the Kennicutt relation is shown in Figure 7a, where we plot $[N(\text{H I}), \dot{\psi}_*]$ pairs for DLAs along with the 1 σ contours of the Kennicutt relation.[4] Clearly the DLAs show no evidence for a Kennicutt relation. Specifically, a Kendall τ test using only positive detections reveals $\tau = 0.25$, and the probability that the null hypothesis of no correlation is correct is $p_{Kendall} = 0.28$. This conclusion differs from the findings of Lanzetta et al. (2002), who used the Kennicutt relation to deduce the SFR intensity distribution as a function of SFR per unit area from the frequency distribution of H I column densities in DLAs. They found excellent agreement with the intensity distribution deduced directly from galaxy brightnesses. In that case $\dot{\psi}_*$ is deduced from emission from pixels with linear dimension of $\approx 0.2 \ h^{-1}$ kpc. By contrast, the H I column densities in DLAs are sampled over transverse distances determined by the linear scale of the continuum source in QSOs, which is typically less than 1 pc. As a result, the agreement between column density measurements on small scales and SFRs per unit area on larger scales indicates that *on average* the Kennicutt relation for nearby galaxies holds in high-z DLAs (Lanzetta et al. 2002).

The reasons why the points in Figure 7a display so much scatter about the Kennicutt relation are straightforward. First, if star formation occurs in the DLA gas, $\dot{\psi}_*$ inferred from the C II* technique is averaged over the linear dimensions of the DLA, which exceed 5 kpc in any model (e.g., Haehnelt, Steinmetz, & Rauch 1998). Because N(H I) likely varies on scales smaller than 5 kpc, correlations between

---

[4] Although the total H column density is used for nearby galaxies, N(H I) is adequate for DLAs where the molecular content of the gas is low (Petitjean, Srianand, & Ledoux 2002; Ledoux, Srianand, & Petitjean 2002).
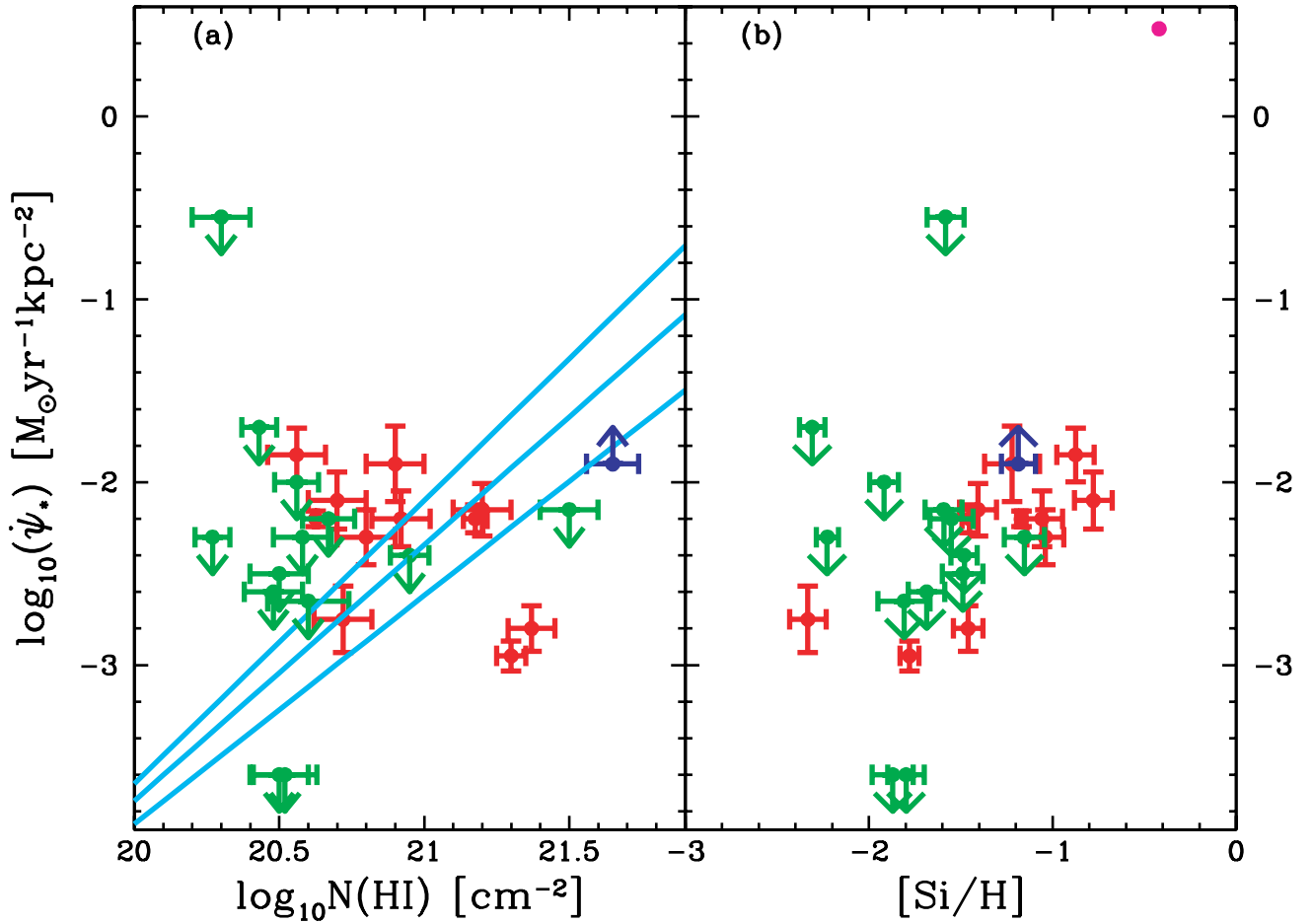
FIG. 7.—(*a*) Comparison between $N(H\;I)$ and $\dot{\psi}_*$ for DLAs with the Kennicutt (1998) relationship defined by $\dot{\psi}_* = [(2.5 \pm 0.7) \times 10^{-4}] \times [N(H\;I)/1.26 \times 10^{20}\;cm^{-2}]^{1.4 \pm 0.15}\;M_\odot\;yr^{-1}\;kpc^{-2}$. Data points inferred with "Gal" dust and minimal depletion. Red data points are positive detections, green are 2 σ upper limits, and blue is 2 σ lower limit. (*b*) Comparison between [Si/H] and $\dot{\psi}_*$. Same color coding as in (*a*). Magenta circle is estimated mean for LBGs.

[$N(H\;I)$, $\dot{\psi}_*$] pairs are not expected. Second, in the bulge model, star formation does not occur in the gas giving rise to damped Lyα absorption. As a result, no correlations between [$N(H\;I)$, $\dot{\psi}_*$] pairs are predicted. However, it may be possible to distinguish between the two models with a sufficiently large data set. If star formation occurs in the DLA gas, $N(H\;I)$ averaged over the DLA sample should correspond to $N(H\;I)$ averaged across a typical DLA; therefore, the sample averages of $N(H\;I)$ and $\dot{\psi}_*$ should obey the Kennicutt relation. On the other hand, no such correlation is predicted for the bulge model. Interestingly, the averages over the positive detections in Figure 7a result in $\langle \dot{\psi}_* \rangle = 6.4 \times 10^{-3}\;M_\odot\;yr^{-1}\;kpc^{-2}$ and $\langle N(H\;I) \rangle = 1.0 \times 10^{21}\;cm^{-2}$, which are within 1 σ of the average Kennicutt relation. In the bulge model this is merely a coincidence.

To search for evidence of feedback, we first looked for correlations between SFR per unit area and metallicity. Nearby spirals exhibit negative radial gradients in metallicity (Garnett et al. 1997) and in SFR per unit area (Dopita & Ryder 1994), implying a correlation between metallicity and SFR per unit area. Such metallicity gradients may have also been detected in DLAs (Wolfe & Prochaska 1998). We used ([Si/H], $\dot{\psi}_*$) pairs to search for such correlations. The results shown in Figure 7b yield tentative evidence for a correlation since $\tau = 0.46$ and $p_{Kendall} = 0.05$, where again we

used only positive detections. We then focused on kinematic evidence for feedback. In the ISM, enhancements in velocity width are found in regions of higher than average SFRs such as Orion (Cowie, Songaila, & York 1979) and Carina (Walborn et al. 1998; Savage, Meade, & Sembach 2001). Evidently, gas in these regions is stirred up by increased supernova activity. We tested for kinematic feedback by looking for correlations between absorption-line velocity width and $\dot{\psi}_*$. Specifically, we checked for kinematic feedback in the neutral gas by searching for correlations between (Δv_{low}, $\dot{\psi}_*$) pairs, where Δv_{low} is the velocity width of low ions in DLAs (PW97). We also checked for kinematic feedback in the ionized gas by searching for correlations between ($\Delta v_{C\;IV}$, $\dot{\psi}_*$) pairs, where $\Delta v_{C\;IV}$ is the velocity width of the C IV $\lambda1550$ transition. The results using only positive detections are shown in Figure 8a and reveal no evidence for correlations in the ionized gas, since $\tau = 0.97$ and $p_{Kendall} = 0.76$. However, Figure 8b does reveal possible evidence for kinematic correlations in the neutral gas, since $\tau = 0.77$ and $p_{Kendall} = 0.002$.

The reasons for null correlations in the case of feedback are the same as discussed above, namely, no correlations are expected for the bulge hypothesis because star formation occurs in regions disconnected from the absorbing gas used to infer metallicity and kinematics. In the disk model, $\dot{\psi}_*$ is averaged over linear scales large
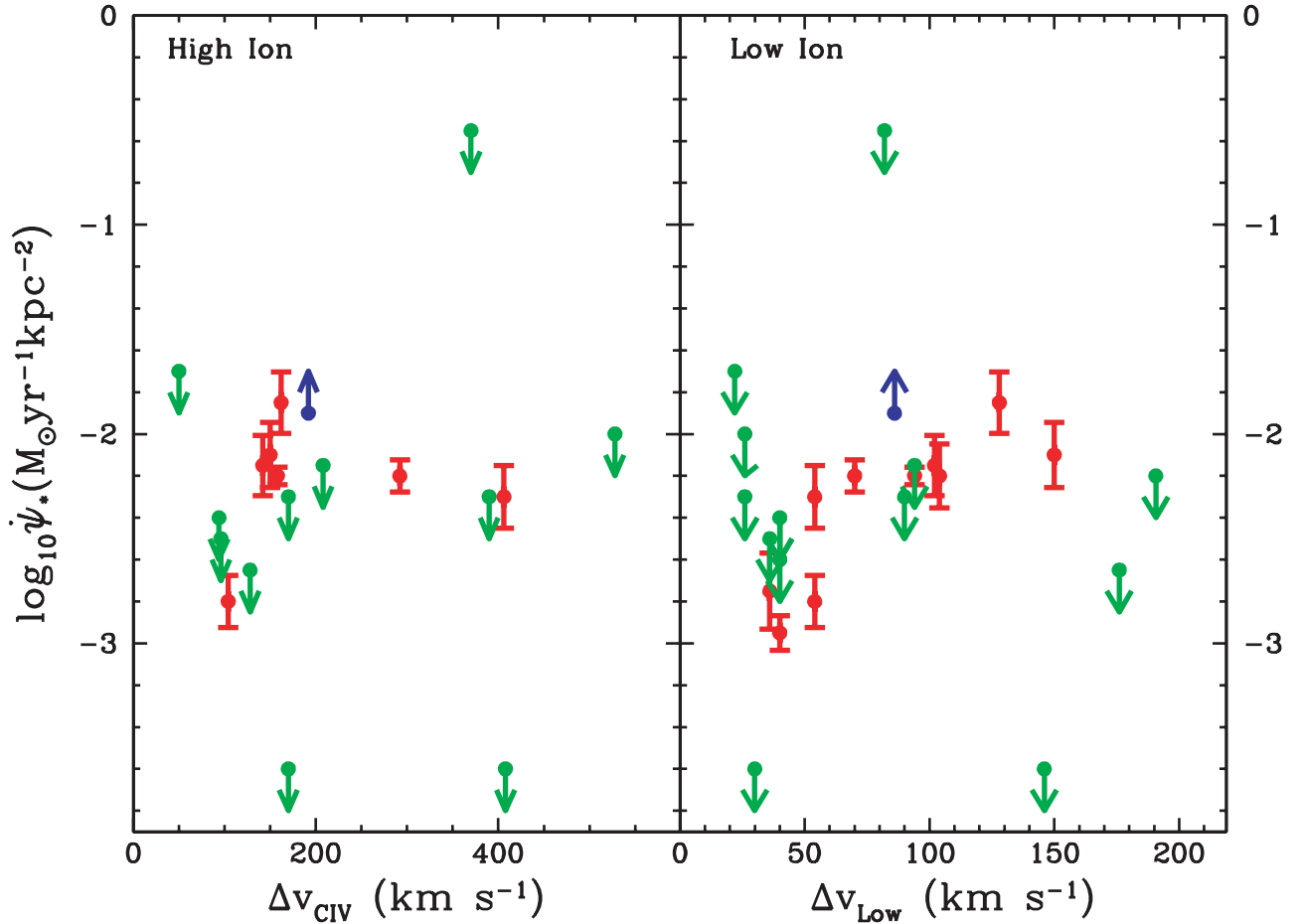
FIG. 8.—(a) Comparison between C IV velocity width $\Delta v_{C\,IV}$ and $\dot{\psi}_*$. (b) Comparison between low-ion velocity width Δv_{low} and $\dot{\psi}_*$. Color coding same as in previous figures.

compared to the ≈ 1 pc transverse dimensions sampled in absorption. Therefore, in this model the null correlation between $\Delta v_{C\,IV}$ and $\dot{\psi}_*$ indicates significant random variations in high-ion velocities on linear scales small compared to the length scale of the star-forming regions in DLAs. Because it is reasonable to expect similar variations in the case of low-ion velocities, how can we understand a correlation between the $(\Delta v_{low}, \dot{\psi}_*)$ pairs, if confirmed? The answer may be that Δv_{low} has global rather than local significance. Specifically, Δv_{low} may reflect the depth of the gravitational potential well of the DLA, as predicted in the case of rotating disks (PW97) or protogalactic clumps (Haehnelt et al. 1998); i.e., the SFR per unit area may be correlated with total mass. Note that this explanation would apply to both the uniform disk and bulge models. A similar explanation might also apply if the tentative correlation between ([Si/H], $\dot{\psi}_*$) pairs is confirmed, namely, that the metallicity of the gas does not vary randomly on scales small compared to scale of the galaxy hosting the DLA. Rather, metallicity might be a function of total mass, as in the case of current galaxies.

Of course, all these results need to be tested with more data. In particular, the statistical significance of the correlation between Δv_{low} and $\dot{\psi}_*$ would be reduced if the two upper limits with greater than 150 km s^{-1} were added to the sample of positive detections. On the other hand, the two

DLAs with $\log_{10} \dot{\psi}_* \approx -3.6$ $M_\odot$ yr^{-1} kpc^{-2} are the "outliers" discussed in § 5.2. These are more likely to be WNM-dominated absorbers with significantly higher values of $\dot{\psi}_*$, in agreement with the predicted correlations.

4. TESTS OF THE MODELS

Having presented evidence for star formation in DLAs and having described the implications of the derived star formation histories, we now discuss three tests of the models upon which these results are based. The first is a test for the grain photoelectric heating mechanism, the second tests the hypothesis that l_c is a cooling rate, and the third describes a search for evidence of a two-phase medium.

4.1. Evidence for Grain Photoelectric Heating

A critical premise of the C II* technique is that neutral gas in DLAs is heated by photoelectrons ejected from interstellar grains by FUV radiation emitted by massive stars. In that case the heating rate per H atom is $\Gamma_d \propto \kappa\epsilon\dot{\psi}_*$. The efficiency of grain photoelectric heating, ϵ, is essentially constant as it is insensitive to variations in electron density, temperature, and FUV radiation field in the CNM. Moreover, the scatter in $\dot{\psi}_*$ is limited such that the average $\log_{10}\langle\dot{\psi}_*\rangle = -2.19^{+0.19}_{-0.26}$ $M_\odot$ yr^{-1} kpc^{-2}. Therefore, a prediction of the grain photoelectric

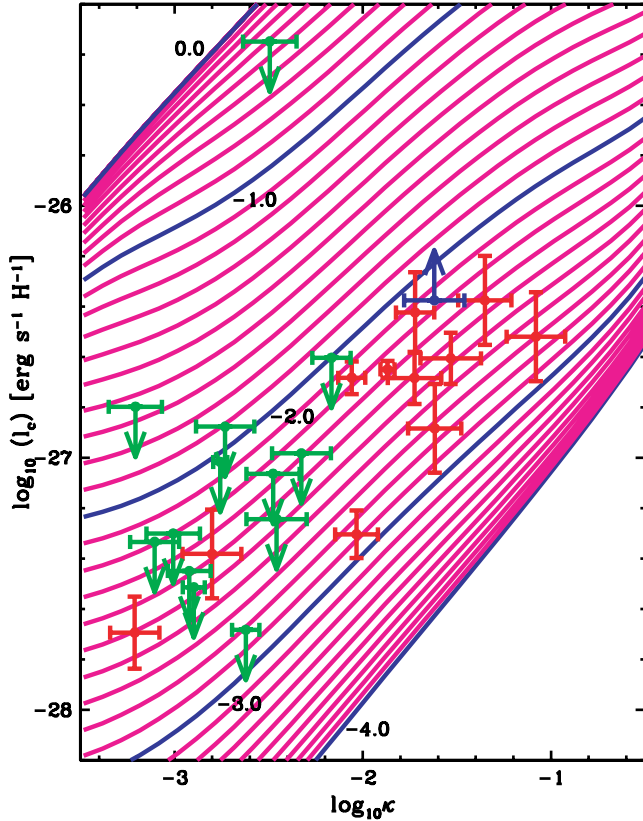FIG. 9.—Plot of dust-to-gas ratio, κ, vs. l_c, where the "Gal" dust and minimal depletion are assumed to compute κ. Color code of data points is the same as in previous figures. Continuous curves are κ vs. l_{cr} relations for constant $\log_{10} \dot\psi_* = -4.0, -3.0, -2.0, -1.0,$ and 0.0 $M_\odot$ yr^{-1} kpc^{-2} predicted by the model described in the text.

heating scenario is that Γ_d should be roughly correlated with the dust-to-gas ratio, κ.

We test the grain photoelectric heating hypothesis by letting $l_c = \Gamma_d$ (which is an excellent approximation in the CNM) and then compare l_c with κ. The two quantities are plotted against each other in Figure 9. The red data points are positive detections, green are upper limits, and blue is a lower limit. The solid curves are lines of constant $\dot\psi_*$ predicted by a version of the CNM model with a fixed redshift and a given prescription for computing κ from metallicity. That is, for a given metallicity and $\dot\psi_*$ we calculate two-phase equilibria of gas subjected to grain photoelectric heating and assume the DLA density to be given by the computed n_{CNM}. We include the CMB contribution to radiative excitations of the [C II] fine-structure states by assuming $z = 2.8$, the median redshift of the sample, and ignore optical pumping (which should lead to no loss in generality since optical pumping is negligible in the CNM). To calculate κ, we adopt the CNM "Gal" model with minimal depletion. As a result, we let the intrinsic carbon abundance be $[C/H]_{int} = [Si/H]_{int} + [Fe/Si]_{int}$ and $[Fe/Si]_{int} = -0.2$. We also assume $[Fe/Si]_{gas} = -0.4$, which is the average value for our sample. We then compute l_{cr} with techniques described in Paper I. Visual inspection of Figure 9 indicates several phenomena. First, the measured l_c and κ are correlated. Specifically, performing the Kendall τ test using the positive detections alone, we find $\tau = 0.64$ and

$p_{Kendall} = 0.0064$, where $p_{Kendall}$ is the probability of the null hypothesis of no correlation. Second, the slope of the data in the (κ, l_c)-plane is approximately parallel to the model predictions, and all the positive detections are bounded by $\log_{10} \dot\psi_* = -2$ and -3 $M_\odot$ yr^{-1} kpc^{-2}. Third, the case for correlation receives additional support from the location of the upper limits at low dust-to-gas ratios, i.e., $\log_{10} \kappa < -2.2$, and the lower limit at the relatively high dust-to-gas ratio, $\log_{10} \kappa > -1.6$.

Can the correlation between l_c and κ be explained by heating mechanisms other than grain photoelectric heating? The obvious alternatives are cosmic-ray and X-ray heating. Suppose that the actual SFRs are orders of magnitude lower than we infer for grain photoelectric heating, but the cosmic-ray ionization rate, ζ_{CR}, is large, i.e., the ratio $\zeta_{CR}/\dot\psi_*$ is orders of magnitude larger than given in equation (9) in Paper I. In that case it is possible for the cosmic-ray heating rate, Γ_{CR}, to dominate the heating rate in the CNM. During ionization by cosmic rays, primary and secondary electrons are mainly liberated from H and He (W95). As a result, Γ_{CR} will be independent of metal abundance and hence independent of κ. Since we have linked ζ_{CR}, and hence Γ_{CR}, to the SFR, and $l_c \approx \Gamma_{CR}$ when cosmic rays dominate, l_c will be independent of κ for a fixed $\dot\psi_*$, in contrast to grain photoelectric heating.

On the other hand, the X-ray heating rate could depend on metallicity, and hence on κ, since abundant heavy elements dominate the X-ray photoionization cross section per H atom at photon energies above the oxygen edge at 0.53 keV (Morrison & McCammon 1983). We used the X-ray heating model of W95, which consists of two local thermal sources with $T \sim 10^6$ K and an extragalactic power-law component. Heating by the thermal sources is dominated by photoionization of H and He since their X-ray spectra cutoff is below 0.53 keV. Although the power-law component extends to energies above the oxygen edge, X-ray heating in this case will also be dominated by photoionization of H and He. The reason is that for typical velocity component column densities, $N(H I) \approx 1 \times 10^{20}$ cm^{-2}, most of the X-rays penetrating the H I gas have energies below 0.53 keV. Photoionization of H and He by these X-rays dominates photoionization of heavy elements by higher energy X-rays as a result of the low metallicities of most DLAs and the shape of the power-law spectrum. Thus, photoionization of heavy elements will not be the dominant source of primary electrons. Consequently, while the condition $l_c \approx \Gamma_{XR}$ might hold in the limit of low SFRs and high X-ray luminosities, Γ_{XR} will be independent of κ for a fixed $\dot\psi_*$.

To conclude, the correlation between l_c and κ is naturally explained by grain photoelectric heating in a CNM. The correlation at a fixed SFR follows from the physics of grain photoelectric heating, while the scatter of l_c at fixed κ reflects the frequency distribution of $\dot\psi_*$. Note that this correlation does not distinguish between the uniform disk and bulge models. Because the heating rate is the product of a "global" quantity, $\dot\psi_*$, and a "local" quantity, κ, clouds with larger κ will have higher heating rates independent of whether the incident FUV radiation arises locally or from the distant bulge. By contrast, neither the cosmic-ray nor X-ray heating rates are correlated with κ at fixed SFR. To explain the observed correlation, one must postulate a correlation between $\dot\psi_*$ and κ (or possibly metallicity). It is

difficult to understand the origins of a correlation between the "global" $\dot{\psi}_*$ and the "local" dust-to-gas ratio in this case.

4.2. Is C II* Excitation Due to the CMB?

Our models predict that in the CNM of most DLAs the cooling rate, $n\Lambda$, equals the spontaneous emission rate of 158 μm radiation, l_c. This condition, $n\Lambda \approx l_c$, holds when the $^2P_{3/2}$ and $^2P_{1/2}$ fine-structure states in the ground term of C^+ are populated by collisional rather than radiative excitations. In Paper I we describe how CMB radiation populates these states directly and how the FUV radiation field, G_0, populates them indirectly through optical pumping via higher energy states. While optical pumping might be important in the WNM, it can be neglected in the CNM. Although an increase in G_0 drives up the pumping rate, it also increases the collisional excitation rate. This is because an increase in G_0, and thus $\dot{\psi}_*$, increases the grain photo-electric heating rate, which raises the CNM density, n_{CNM}, as shown in Figure 5 in Paper I. As a result, the ratio of collisional to optical pumping rates always exceeds unity in the CNM.[5] This need not be true for the ratio of collisional to CMB excitation rates because the CMB does not heat the CNM gas (through Compton heating) in the redshift range of our sample DLAs. Because the value of n_{CNM} does not rise with increasing CMB intensity, the CMB may dominate collisions as a source of excitation in DLAs with low values of n_{CNM} and high redshifts where the CMB intensity is high.

Because the balance between collisional and CMB excitations depends on various assumptions included in our models, it is important to assess their relative importance with model-independent tests. Figure 10 illustrates the results of a test relying on one free parameter, the carbon abundance, (C/H). Here we plot l_c, inferred from measurements of $N(C II^*)$, versus redshift for a sample of 30 DLAs. For each DLA we also plot, as magenta stars, $(l_c)_{CMB}$ versus redshift where $(l_c)_{CMB}$ is the value assumed

[5] Although the density of the WNM, n_{WNM}, also increases with G_0, the densities are not high enough for collisions to dominate optical pumping in most cases.

by l_{cr} when the CMB is the only source of excitation and de-excitation (in Paper I we showed that $(l_{cr})_{CMB} = 2(C/H)A_{ul}h\nu_{ul}\exp\{-h\nu_{ul}/[k(1+z)T_{CMB}]\}$). A total of 25 of the DLAs are drawn from the minimal depletion sample. Here we calculate $(l_c)_{CMB}$ by assuming [C/H] = [Si/H] − 0.2 to compute (C/H). The plot also shows data for five additional DLAs. They include the DLAs toward Q0201+11 and Q2344+12 for which we assumed maximal depletion to obtain (C/H) because [Fe/Si] > −0.2 in both DLAs. We also included the DLAs toward Q0951−04, Q1425+60, and Q1443+27 for which we assumed [C/H] = [Si/H] − 0.2. These objects were excluded from the original minimal depletion sample because observational limits on [Si/H] or [Fe/H] prevented us from computing the dust-to-gas ratio, κ, which is not needed to compute $(l_c)_{CMB}$.

The figure demonstrates that the CMB cannot explain the observed level of C II* excitation for the following reasons. First, despite the dispersion in carbon abundance, $(l_c)_{CMB}$ should increase rapidly with increasing redshift, whereas the observed values of l_c show no dependence on redshift in the interval $z = [1.6, 4.5]$. Second, with two exceptions, the CMB excitation rate is too low to explain the observations. This is true even at $z > 3$ where the predicted values of $(l_c)_{CMB}$ merge with the observed spontaneous emission rates.

The exceptions are the DLAs at $z = 3.608$ and 4.080 toward Q1108−07 and Q2237−06, the "outliers" discussed in Paper I. In these DLAs, $(l_c)_{CMB}$ comprises a significantly higher fraction (>0.8) of l_c than for the other DLAs. Because the l_c values are upper limits, the data place lower than usual upper limits on the [C II] 158 μm cooling rates. We interpreted this to mean that these sight lines pass only through WNM gas subjected to SFRs within the range determined from the CNM hypothesis. However, we cannot rule out the possibility that the gas is subjected to negligible SFRs, which lead to gas densities so low that collisional excitations are unimportant. In that event, CMB excitation alone would be responsible for the observed l_c. To decide between these hypotheses, we need to measure l_c and $(l_c)_{CMB}$ more accurately. Although l_c can be determined more precisely through better measurements of the C II* $\lambda1335.7$ velocity profiles, higher signal-to-noise ratio will not improve the accuracy of $(l_c)_{CMB}$ where the only source of error is in determining (C/H). The carbon abundance is difficult to obtain directly because the principal C II transitions are always saturated (e.g., Dessauges-Zavadsky et al. 2001). Instead we compute $(l_c)_{CMB}$ with the minimal depletion assumption, [C/H] = [Si/H] + [Fe/Si]$_{int}$ and [Fe/Si]$_{int}$ = −0.2, for 28 of the 30 data points shown in Figure 11. For the remaining two DLAs, [Fe/Si]$_{gas}$ > −0.2, which violates the nucleosynthetic ceiling limit in the minimal depletion model, and we thus assume [Fe/Si]$_{int}$ = 0, i.e., maximal depletion. We favor minimal depletion for most DLAs because it leads to self-consistent determinations of $(l_c)_{CMB}$, whereas maximal depletion leads to the inconsistent condition $(l_c)_{CMB} > l_c$ for the Q1108−07 and Q2237−06 DLAs. In any case the limited accuracy for determining (C/H) results in errors in $(l_c)_{CMB}$ of order 0.2 dex, which is inadequate for distinguishing collisional excitation from CMB excitation.

In our treatment of CMB excitations of the C II fine-structure states we assume the CMB temperature at redshift z to be $T_{CMB}(z) = (1+z)T_{CMB}$, whereas most published
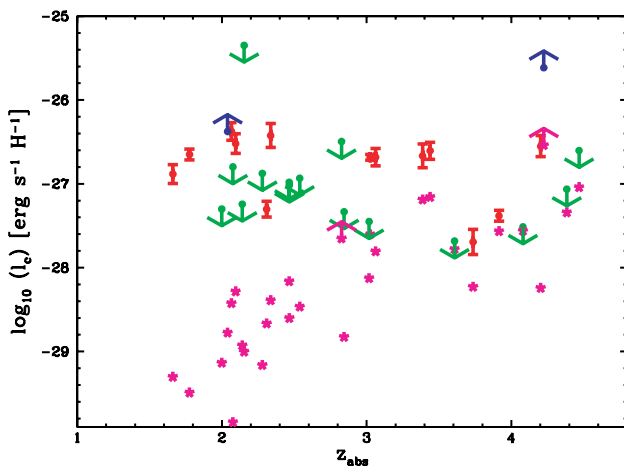

FIG. 10.—Plot of l_c vs. redshift. Red, green, and blue filled circles have usual meanings. Magenta stars depict $(l_c)_{CMB}$ corresponding to measurements of l_c at each redshift. The plot shows data for 30 DLAs. Computation of $(l_c)_{CMB}$ is explained in the text.

Fig. 11.—Comparison between C II* and resonance-line velocity profiles for three DLAs. Top row of panels shows profiles for C II* λ1335.7. Second row shows profiles for Si II λ1808, and third row for (*a*) Fe II λ1608 and (*b*) and (*c*) Ni II λ1741. Bottom row shows $\log_{10}[(\mathcal{R} - \langle\mathcal{R}\rangle)/\langle\mathcal{R}\rangle]$ computed for successive 20 km s^{-1} bins where $\mathcal{R}$ is the ratio of C II* λ1335.7 to resonance-line optical depth. (*a*), (*b*), and (*c*) show data for DLAs toward Q0347−08, Q0100+13, and Q2231−00.

treatments *test* this assumption by attempting to measure $T_{\rm CMB}(z)$ directly. In principle, this can be done by first making independent estimates of the collisional contribution to the level populations of the $^2P_{3/2}$ and $^2P_{1/s}$ fine-structure states and then computing the blackbody temperature required to explain the observed population ratio (e.g., Molaro et al. 2002). Accurate UVES echelle spectra were acquired by the VLT for two DLAs in our sample: Q0347−38 (Levshakov et al. 2002; Molaro et al. 2002) and

Q1232+08 (Srianand et al. 2000). In Table 2 we compare physical parameters obtained by these authors with predictions of our CNM models. The estimates are independent of our predictions because physical models of the DLA gas were not constructed. Rather, techniques such as measuring velocity line widths to estimate the kinetic temperature or inferring G_0 from the fractional abundance of H_2 were used. In some cases relative abundances of various rotational levels of H_2 were used to infer the temperature, and the ratio

TABLE 2
PHYSICAL PARAMETERS FOR DLA GAS

PARAMETER	Q1232+08		Q0347−38	
	Estimate[a]	CNM Model[b]	Estimate[c]	CNM Model[b]
n (cm^{-3})	20–335	7–14	4–14	3–6
T (K)	85–285	130–188	<950[d]	130–200
n_e (cm^{-3})	0.02	0.002–0.03	...	0.002–0.014
G_0	∼1.7[e]	6.0–21.5	∼ 1.7[e]	2.7–11.0

[a] From Srianand et al. 2000.
[b] Parameter range predicted by CNM models with "Gal" and "SMC" dust and minimal and maximal depletion.
[c] From Levshakov et al. 2002.
[d] Upper limit from velocity dispersion $\sigma = 1.4$ km s^{-1} observed for H_2 lines differs from estimate of Levshakov et al. 2002.
[e] Inferred from reported photoabsorption rate in Lyman and Werner bands, β_0.

Mg^+/Mg^0 was combined with G_0 and photoionization equilibrium to obtain n_e. The results in Table 2 show, with the possible exception of G_0, reasonable agreement between our predictions and these estimates. They are also inconsistent with our WNM model for both DLAs.

4.3. Ratios of C II* to Resonance-Line Velocity Profiles: Probing the Two-Phase Medium

Here we discuss an observational test of the two-phase medium, a key element in our models of DLAs. We describe various aspects of the test and leave more quantitative analyses for future discussions. Note that Lane, Briggs, & Smette (2000) provide independent evidence for a two-phase medium from their analysis of 21 cm absorption in a DLA with $z = 0.0912$.

Suppose, by analogy with the ISM, that the probabilities that the line of sight intercepts WNM and CNM clouds are comparable (Kulkarni & Heiles 1987). If velocity components (i.e., clouds) in each phase have comparable H I column densities and the same element abundances, then a random sight line through a typical DLA should encounter similar column densities of metals in each phase. This can lead to measurable differences between the velocity profiles of C II* $\lambda1335.7$ and resonance transitions such as Si II $\lambda1808.0$, as we now show.

Consider a two-phase configuration in which the fractions y_{CNM} and y_{WNM} of the total $N(\text{H I})$ are in the CNM and WNM, where $y_{\text{CNM}} + y_{\text{WNM}} = 1$. Assume the systemic cloud velocities to be u_{CNM} and u_{WNM} and the internal Gaussian velocity dispersions to be σ_{CNM} and σ_{WNM}. In that case the optical depths at velocity v in C II* $\lambda1335.7$ and Si II $\lambda1808.0$ are given by

$$\tau_v = \frac{\pi e^2}{mc} \frac{1}{\sqrt{2\pi}} N(\text{H I})$$

$$\times \begin{cases} f_{\text{C II*}}\lambda_{\text{C II*}} \dfrac{(l_c)_{\text{CNM}}}{A_{ul}h\nu_{ul}} \left[y_{\text{CNM}} \dfrac{\Phi(v - u_{\text{CNM}})}{\sigma_{\text{CNM}}} \right. \\ \qquad \left. + y_{\text{WNM}} \dfrac{(l_c)_{\text{WNM}}}{(l_c)_{\text{CNM}}} \dfrac{\Phi(v - u_{\text{WNM}})}{\sigma_{\text{WNM}}} \right] \quad \text{for C II*}, \\[2ex] f_{\text{Si II}}\lambda_{\text{Si II}} \left(\dfrac{\text{Si}}{\text{H}}\right) \left[y_{\text{CNM}} \dfrac{\Phi(v - u_{\text{CNM}})}{\sigma_{\text{CNM}}} \right. \\ \qquad \left. + y_{\text{WNM}} \dfrac{\Phi(v - u_{\text{WNM}})}{\sigma_{\text{WNM}}} \right] \quad \text{for Si II}, \end{cases}$$

$$(11)$$

where we used equation (3) in Paper I to compute $\tau_v(\text{C II*})$, the f- and λ-values are oscillator strengths and transition wavelengths, $(l_c)_{\text{CNM}}$ and $(l_c)_{\text{WNM}}$ are l_c in the CNM and WNM, $\Phi(v)$ is the velocity profile normalized such that $\int \Phi(v) d(v/\sqrt{2\pi}\sigma) = 1$, and (Si/H) is the Si abundance.

To compute $(l_c)_{\text{CNM}}$ and $(l_c)_{\text{WNM}}$, we evaluate l_c at the phase densities n_{CNM} and n_{WNM}. Equation (11) in Paper I shows that $l_c = n\Lambda_{\text{C II}} + (l_c)_{\text{pump}} + (l_c)_{\text{CMB}}$, where $n\Lambda_{\text{C II}}$ is the net loss of thermal energy due to 158 μm emission and $(l_c)_{\text{pump}}$ and $(l_c)_{\text{CMB}}$ are the spontaneous energy emission rates in the limits of pure optical pumping and CMB excitation, which are defined in equation (12) in Paper I. At the high values of n_{CNM}, the fine-structure states are mainly populated by collisions, and as a result l_c equals the cooling rate $n\Lambda_{\text{C II}}$, which equals the grain photoelectric heating rate

in the CNM, i.e.,

$$(l_c)_{\text{CNM}} = \Gamma_d. \quad (12)$$

However, at the low values of n_{WNM} any one of the three terms in the above equation for l_c can dominate. For example, $(l_c)_{\text{WNM}} \approx (l_c)_{\text{CMB}}$ in the $z = 3.736$ DLA toward Q1346$-$03 for the CNM solution in which $G_0 = 1.95$. By contrast, $(l_c)_{\text{WNM}} \approx (l_c)_{\text{pump}}$ in the $z = 2.039$ DLA toward Q0458$-$02 for the CNM solution in which $G_0 > 13.5$ (see Fig. 5 in Paper I). Without optical pumping, $(l_c)_{\text{WNM}} \approx n\Lambda_{\text{C II}}$ if the metallicity is low and observed l_c is high. In this case l_c does not equal Γ_d because [C II] emission is *not* the dominant coolant. If $(l_c)_{\text{WNM}}$ is governed by optical pumping, the ratio $(l_c)_{\text{WNM}}/(l_c)_{\text{CNM}}$ is rather well determined because the quantities Γ_d and Γ_{ul} are proportional to both the radiation intensity G_0 and metallicity. Combining the last equation with equations (1) and (7) in Paper I and assuming $[\text{C/H}]_{\text{gas}} = [\text{Si/H}] + [\text{Fe/Si}]_{\text{int}}$, we find

$$\frac{(l_c)_{\text{WNM}}}{(l_c)_{\text{CNM}}} = 7.5 \times 10^9 \frac{(\text{C/H})_\odot (\Gamma_{lu})_{\text{ISM}}}{(1 - 10^{[\text{Fe/Si}]_{\text{gas}} - [\text{Fe/Si}]_{\text{int}}})\epsilon_{\text{CNM}}}, \quad (13)$$

where $(\Gamma_{lu})_{\text{ISM}}$, the optical pumping rate corresponding to the Draine (1978) radiation field, equals 1.57×10^{-10} s^{-1} (Silva & Viegas 2002) and ϵ_{CNM} is the heating efficiency in the CNM. In deriving the last equation we assume that the pumping rate corresponding to intensity G_0 is given by $\Gamma_{lu}(G_0) = (\Gamma_{lu})_{\text{ISM}}(G_0/1.7)$. Averaging over the positive detections in the "Gal" minimal depletion model, we find the average ratio $\langle (l_c)_{\text{WNM}}/(l_c)_{\text{CNM}} \rangle = 0.097 \pm 0.020$ with optical pumping and $\langle (l_c)_{\text{WNM}}/(l_c)_{\text{CNM}} \rangle = 0.067 \pm 0.011$ without pumping. As a result, equation (11) implies that the WNM is undetectable in C II* $\lambda1335.7$ for any value of y_{WNM} but is detectable in resonance transitions such as Si II $\lambda1808.0$ for $y_{\text{WNM}} > 0.1$. Consequently, a significant decrease in $\tau_v(\text{C II*})/\tau_v(\text{Si II})$ from the mean would signify the presence of the WNM.

Such variations may have been detected in the DLA toward Q0347$-$38. Although Figure 11a shows clear evidence for distinct velocity components at $v = -8$ km s^{-1} and $v = +12$ km s^{-1} in Si II $\lambda1808$ and Fe II $\lambda1608$, the $v = -8$ km s^{-1} component is not seen in C II* $\lambda1335.7$. Rather, an asymmetric blue wing extends from $v = +12$ km s^{-1} to $v = -20$ km s^{-1}. Because some of this absorption is due to weak C II* $\lambda1335.66$ ($f_{1335.66}/f_{1335.71} = 0.11$), the observed optical depth of the wing places an upper limit on $\tau_v(\text{C II*}\ \lambda1335.71)$. Therefore, we conjecture that the $v = -8$ km s^{-1} component consists of WNM gas, while the $v = +12$ km s^{-1} component consists of CNM gas. The presence of H_2 absorption only at $v = +12$ km s^{-1} and the lower S^+/N^0 ratio in this component (Levshakov et al. 2002) supports this interpretation. Notice that the relative optical depths of these two components in Fe II $\lambda1608$ are different than in Si II $\lambda1808$. The most likely explanation is enhanced Fe depletion in the $v = +12$ km s^{-1} component. This does not affect our interpretation of the C II* profile because enhanced depletion at $v = +12$ km s^{-1} cannot explain the weakness of C II* $\lambda1335.7$ at $v = -8$ km s^{-1}. In any case the significant decrease in the ratio $\mathcal{R}(v) \equiv \tau_v(\text{C II*})/\tau_v(\text{Si II})$, with decreasing velocity shown in the fourth panel of Figure 11a, is naturally explained by the presence of WNM gas at negative velocities.

Figure 11b compares C II* and resonance-line profiles for the DLA toward Q0100+13 (PHL 957). By contrast with

Figure 11a, the C II* profile in this case closely resembles the Si II λ1808 and Ni II λ1741 profiles. The only significant difference is at $v < -8$ km s^{-1}, where C II* λ1335.71 exhibits a blue asymmetric wing that is missing from Si II λ1808 and Ni II λ1741. We believe this is a blend with weak $v = 0$ absorption in C II* λ1335.66. Because we ignore the increased C II* absorption at $v > +30$ km s^{-1}, which is likely to be a blend with Lyα forest absorption lines, we find no compelling evidence for a WNM in this DLA. However, this does not rule out the presence of a WNM. Suppose that the velocity components at $v \approx +3$ and $+15$ km s^{-1} each contain WNM and CNM gas with the same velocity dispersion. From equation (11) we see that the ratio $\mathcal{R}(v)$ will not vary with v. However, in a scenario where the multiphase structure resembles that of the ISM, the Si II velocity profiles would be wider than the C II* profile, since $\sigma_{WNM} \approx 2\sigma_{CNM}$ in the ISM (Kulkarni & Heiles 1987). In principle, this is a signature of the WNM, but differences between the *observed* profiles will be diluted by the finite resolution of HIRES (FWHM $\approx$ 7–8 km s^{-1}), which is comparable to the widths of most components (i.e., they are unresolved), and Poisson noise. A detailed evaluation of these effects will be discussed elsewhere.

Figure 11c compares C II* and resonance-line profiles for the DLA toward Q2231−00. Although the profiles are noisier in this case, some effects are clear. First, the ratio $\mathcal{R}(v)$ does not exhibit significant variations at $v < -60$ km s^{-1}. On the other hand, there is evidence for variations of $\mathcal{R}(v)$ in the component centered at $v = 0$ km s^{-1}. At $v \approx +10$ km s^{-1}, $\mathcal{R}(v)$ is lower than $\langle \mathcal{R} \rangle$, the mean $\mathcal{R}(v)$ integrated over the entire profile (see the fourth panel of Fig. 12c). This is consistent with WNM gas at $v \approx +10$ km s^{-1}. At the same time, there is tentative evidence for enhanced C II* absorption between $v \approx -30$ and -10 km s^{-1} where C II* λ1335.71 exhibits stronger absorption than either Si II λ1808 or Ni II λ1741. While weak C II* λ1335.66 absorption at $v \approx 0$ km s^{-1} may cause the excess C II* λ1335.71 absorption at $v \geq -10$ km s^{-1}, it cannot explain the excess C II* λ1335.71 absorption at $v < -10$ km s^{-1}.

Excess C II* absorption can be due to increased heating of the CNM. In the case of absorption by CNM gas alone we have

$$\mathcal{R}(v) \equiv \frac{\tau_v(\mathrm{C\ II}^*)}{\tau_v(\mathrm{Si\ II})} = \left(\frac{f_{\mathrm{C\ II}^*}\lambda_{\mathrm{C\ II}^*}}{f_{\mathrm{Si\ II}}\lambda_{\mathrm{Si\ II}}} \frac{1}{h\nu_{ul}A_{ul}} \right) \left[\frac{10^{-24}\kappa\epsilon G_0}{(\mathrm{Si/H})} \right], \quad (14)$$

where we combined the definition of Γ_d (eq. [1] in Paper I) and equation (12). Detectable variations in $\mathcal{R}(v)$ in CNM gas are most likely caused by variations in ϵ and G_0 rather than in absolute element abundances. This is because

$$\frac{\kappa}{(\mathrm{Si/H})} = \frac{(10^{[\mathrm{Fe/Si}]_{int}} - 10^{[\mathrm{Fe/Si}]_{gas}})}{(\mathrm{Si/H})_\odot}, \quad (15)$$

and the recent analysis by Prochaska (2003) showed evidence for remarkable uniformity in the *relative* abundances of DLAs (with the exception of the DLA toward Q0347−38). As a result,

$$\delta_{\mathcal{R}}(v) = \frac{\epsilon(v)G_0(v) - \langle \epsilon G_0 \rangle}{\langle \epsilon G_0 \rangle}, \quad (16)$$

where $\delta_{\mathcal{R}}(v) = [\mathcal{R}(v) - \langle \mathcal{R} \rangle]/\langle \mathcal{R} \rangle$ and $\epsilon(v)$ and $G_0(v)$ are the grain photoelectric heating efficiency and FUV mean intensity at velocity v. Because ϵ is a function of $G_0\sqrt{T}/n_e$ (Bakes & Tielens 1994; Weingartner & Draine 2001), $\delta_{\mathcal{R}}(v)$ will vary with v if any one of these parameters changes with v. If $G_0\sqrt{T}/n_e \ll 5 \times 10^3$ K$^{1/2}$ cm^3, the grains are mainly neutral and ϵ is insensitive to variation in G_0. Therefore, in this CNM limit, $\delta_{\mathcal{R}}(v) \approx \Delta G_0/G_0$. The excess C II* absorption in the Q2231−00 DLA can then result from the incidence of a larger than average radiation intensity, G_0, on the CNM gas in the velocity range $v = -30$ to -10 km s^{-1}. Spatial variations in radiation intensity along the line of sight could result from (1) nearer than average displacement of OB stars from this gas, (2) differing CNM cloud distances from a centrally located bulge source, or (3) passage of the line of sight through separate protogalactic clumps with independent SFRs, in the case of CDM galaxy formation scenarios (Haehnelt et al. 1998). The CDM scenario should produce standard deviations, $\sigma_{\delta_{\mathcal{R}}} \approx 1$, because the SFRs would be uncorrelated at the different clump locations. However, in the bulge scenario, we find $\Delta G_0/G_0 \sim h/b$, where h is the thickness of the surrounding disk and b is the sight-line impact parameter. This would lead to $\sigma_{\delta_{\mathcal{R}}} < 1$ for typical values of b. To discriminate between these hypotheses, larger samples of DLAs with measured $\mathcal{R}(v)$ are required.
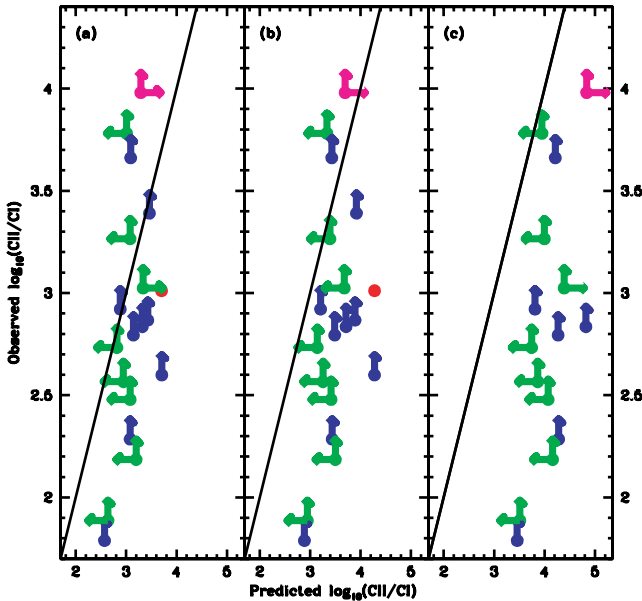

FIG. 12.—Plot of observed vs. predicted C II/C I ratios for 19 DLAs from Table 1. With the exception of the filled red circle, which is a positive detection, the *observed* C II/C I ratios are lower limits. The filled blue circles correspond to DLAs for which we have positive detections of l_c. Filled green circles correspond to DLAs with limits on l_c, and the filled magenta circle corresponds to DLA with lower limit on l_c (see text). (a) Results for model with $\log_{10} N_w = 19.3$ cm^{-2} and standard ratio of $\zeta_{CR}/\dot{\psi}_*$ (eq. [9] in Paper I). (b) Same as (a), except $\log_{10} N_w = 20$ cm^{-2}. (c) Same as (b), except $\zeta_{CR}/\dot{\psi}_*$ equals 0.3 times the standard ratio.

5. DO HIGH-z DLAs CONTAIN CNM GAS?

In this section we discuss possible objections to the presence of CNM gas in DLAs. Recall that if C II* λ1335.7 absorption arises in WNM gas, the inferred FUV radiation contributes more background radiation than observed. On the other hand, if it arises in CNM gas, the background

radiation is consistent with observations. Nonetheless, the following arguments have been made against the presence of CNM gas in high-z DLAs.

5.1. C II/C I Ratios

The first of these has to do with the large values observed for the ratio $N(\text{C II})/N(\text{C I})$ (hereafter C II/C I). Liszt (2002) constructed two-phase models similar to ours and computed C II/C I ratios for five DLAs for which observed ratios were available. While the ratios he predicted for the CNM were lower than observed, those predicted for the WNM were consistent with observed values. He concluded that the observed C II/C I ratios permit no more than a few percent of the DLA gas to be in the CNM phase.

We repeated these calculations with the CNM model with "Gal" dust and minimal depletion. In Figure 12 we compare the results with C II/C I ratios deduced for 19 DLAs in our sample. With the exception of the filled red circle depicting a positive detection, the *observed* C II/C I ratios are lower limits, while the *predicted* C II/C I ratios are definite numbers if l_c is detected (*filled blue circles*), and upper or lower limits if limits are placed on l_c (*filled green circles*; see caption to Fig. 12). Figure 12a shows results for a model incorporating many of the assumptions made by Liszt (2002). In particular, we assume that the incident soft X-ray radiation is attenuated by gas with H I column density $\log_{10} N_w = 19.3$ cm^{-2}. We are in general agreement with Liszt (2002) that this CNM model cannot account for the large values observed for C II/C I. Although the model predictions should lie to the right of the diagonal line representing equality between observed and predicted ratios, one-third of the sample is on or to the left of the line. This disagreement takes on significance when it is realized that all the discrepant points are lower limits on the observed C II/C I ratio and hence the actual ratios are displaced even further from agreement with model predictions.

However, the predicted C II/C I ratios are sensitive to changes in model input parameters. This is evident in Figure 12b, showing results for the same model as in Figure 12a except N_w is increased to 10^{20} cm^{-2}, i.e., to the attenuating column density, which is more appropriate for DLAs and is used in all our calculations (see discussion in Paper I). Comparison with Figure 12a reveals an increase in predicted C II/C I ratios by ~0.4 dex with a consequent improvement between theory and observation. The reasons for the increase in C II/C I are as follows. The increase in N_w results in a reduction in X-ray intensity, which in turn causes a decrease in the heating rate. This decreases the gas pressure, which brings about a decrease in the CNM density, n_{CNM}, as illustrated in Figure 5 in Paper I. For a given l_c a decrease in n_{CNM} causes an increase in $\dot{\psi}_*$ (and hence G_0), a decrease in n_e, and a rise in T. All three factors conspire to increase the C II/C I ratio, since it is proportional to $G_0/[n_e \alpha_{\text{C I}}(T)]$, where $\alpha_{\text{C I}}(T)$, the case A recombination coefficient to C I, decreases with increasing T. For many DLAs even better agreement is achieved if we retain $\log_{10} N_w = 20$ cm^{-2} and reduce the ratio of cosmic-ray ionization rate to SFR per unit area, $\zeta_{\text{CR}}/\dot{\psi}_*$, below the ratio given in equation (9) in Paper I. At these low X-ray intensities, cosmic rays still dominate the ionization rate, and as a result n_{CNM} is reduced even further. Figure 12c shows results for $\zeta_{\text{CR}}/\dot{\psi}_*$ equaling 0.3 times the ratio in equation (9) in Paper I. In this case most of the predicted C II/C I ratios are in better agreement

with observations than before. However, in the most metal-rich DLAs the additional decrease in pressure accompanying the reduction in $\zeta_{\text{CR}}/\dot{\psi}_*$ results in the disappearance of the pressure maxima and minima essential for two-phase equilibria. This is why four of the DLAs in Figures 12a and 12b are missing from Figure 12c. Clearly, more realistic models might include a range in $\zeta_{\text{CR}}/\dot{\psi}_*$ ratios rather than assigning the same value to each DLA.

The point of this exercise is to show that the C II/C I ratio depends sensitively on the X-ray and cosmic-ray ionization rates, both of which are uncertain. For these reasons, it is premature to use the C II/C I ratio to rule out CNM gas in DLAs. On the other hand, the observed C II/C I ratios are useful for placing upper limits on the $\zeta_{\text{CR}}/\dot{\psi}_*$ ratio. We find that $\zeta_{\text{CR}}/\dot{\psi}_*$ in our model CNM gas cannot be more than 2 times the value in equation (9) in Paper I. Otherwise, more than one-third of the points in Figure 12 would lie above the diagonal line.

5.2. Equilibrium Gas Pressures in DLAs

The second argument against CNM gas in high-z DLAs was made by Norman & Spaans (1997). They concluded that high-z DLAs instead consisted of pure WNM gas with pressures $P < P_{\text{min}}$. Computing two-phase equilibria in the context of CDM models for galaxy formation, they found that at $z > 1.5$ the gas equilibrium pressure, P_{eq}, exceeded the hydrostatic pressure, P_{hydro}, in the midplanes of protogalactic disks embedded in dark matter halos. By contrast, P_{eq} was predicted to be less than P_{hydro} at $z < 1.5$. They concluded that the hydrostatic pressure available in model protogalaxies is insufficient to generate two-phase media at $z > 1.5$. The ratio $P_{\text{hydro}}/P_{\text{eq}}$ decreases with increasing redshift because P_{eq} increases as a result of the sharp decline of metallicity with redshift predicted by Norman & Spaans (1997).

We tested these predictions using measurements of l_c to infer P_{eq}. The results shown in Figure 13 were obtained with the CNM, "Gal" dust, minimal depletion model discussed above. In Figure 13a we plot P_{eq} versus z. The average of the pressures corresponding to the positive detections is $P_{\text{eq}}/k = (1.33 \pm 0.81) \times 10^3$ K cm^{-3}. This is much lower than the gas pressures predicted by Norman & Spaans (1997), which exceed ~10^5 K cm^{-3} at $z > 1.5$ (see their Fig. 3), but in agreement with P_{hydro} predicted for typical CDM models. According to the CDM models of Mo, Mao, & White (1998), two-thirds of DLAs detected in absorption at $z \approx 2.5$ should arise in halos with circular velocities, $V_c > 100$ km s^{-1}. Using the Norman & Spaans (1997) formalism, we find the corresponding hydrostatic pressures to exceed 2×10^3 K cm^{-3}. Given the uncertainties, we conclude that the hydrostatic pressures available in CDM models are sufficient to generate the type of two-phase equilibria we infer for DLAs. Coincidentally, these pressures could also arise in high-z DLAs if they resemble nearby massive galaxies such as the Milky Way where the gas pressures at the solar circle are $\approx 3 \times 10^3$ K cm^{-3} (Wolfire et al. 2003). The analysis of Mo et al. (1998) and Norman & Spaans (1997) shows $P_{\text{hydro}} \propto [V_c H(z)]^2$, where the Hubble parameter $H(z)$ is an increasing function of redshift. Therefore, low-mass objects at high redshift can in principle generate as much hydrostatic pressure as high-mass objects with low redshifts. As a result, pressure does not discriminate between DLA models based on CDM from the null
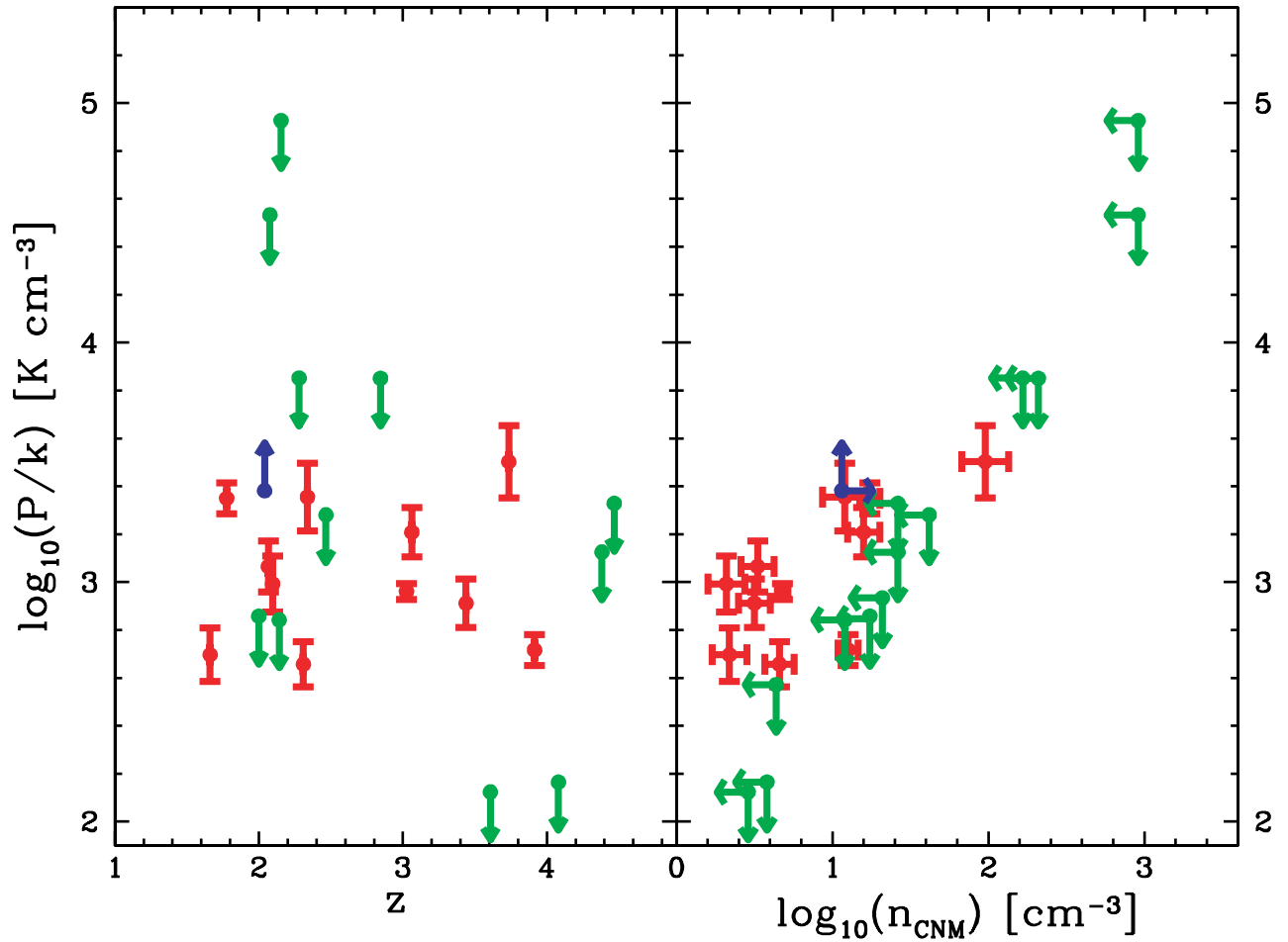
Fig. 13.—Plot showing equilibrium pressure [i.e., $(P_{min}P_{max})^{1/2}$] vs. z and n_{CNM}. Pressures computed for standard CNM model with "Gal" dust and minimal depletion. (*a*) Plot of P/k vs. z. Two upper limits at $\log_{10}(P/k) < 2.2$ K cm^{-3} correspond to DLAs along sight lines toward Q1108−07 and Q2237−06, which probably encounter only WNM gas. In that case the pressures would be higher than shown. (*b*) Plot of P/k vs. n_{CNM}.

hypothesis in which DLAs are the unevolved disks of current normal galaxies (e.g., PW97), nor does the absence of redshift evolution evident in Figure 13*a*. This is an obvious prediction of the null hypothesis. In the case of CDM we note that the nonlinear mass scale $M_c \propto (1+z)^{-[6/(n+3)]}$, where n is the power spectrum index (Padmanabhan 1993, p. 335), and the virial velocity $V_c \propto [H(z)M_c(z)]^{1/3}$, where the Hubble parameter $H(z) \propto (1+z)^{3/2}$ for the Einstein–de Sitter cosmology. Since $n = -2$ at galactic scales, P_{hydro} is independent of redshift. As a result, the redshift dependence of P_{hydro} is negligible in both models.

In Figure 13*b* we plot P_{eq} versus CNM density, n_{CNM}. The densities corresponding to positive detections (*red data points*) range between 2 and 100 cm^{-3} with an average $\langle n_{CNM} \rangle = 16$ cm^{-3}. These resemble densities inferred for the CNM clouds in the Galaxy (W95). Because the H I column density of a typical DLA velocity component is approximately 1×10^{20} cm^{-2} (PW97), the volume densities imply physical dimensions on the order of a few parsecs. This conclusion differs from arguments that DLA clouds causing 21 cm absorption uniformly cover the cores of compact radio sources that typically have linear sizes of ∼100–400 pc (Briggs & Wolfe 1983) and has important implications for interpreting measurements of 21 cm absorption in DLAs (see § 5.3). The linear correlation evident in Figure 13*b* is

tentative because the Kendall τ test for positive detections indicates $\tau = 0.45$ and the probability for the null hypothesis of no correlation of $p_{Kendall} = 0.052$. We find the average temperature $\langle T \rangle = 190 \pm 130$ K for this model. The temperatures are higher than diffuse clouds in the ISM as a result of the combination of low densities and low metallicities.

5.3. *High Spin Temperatures at Large Redshifts*

The third argument against CNM gas at high redshifts stems from the high spin temperatures, T_s, deduced from 21 cm absorption observations of DLAs. Whereas spin temperatures in nearby spirals are less than 300 K (Dickey & Lockman 1990), the spin temperatures in most DLAs exceed 500 K (Chengalur & Kanekar 2000). The discrepancy is greatest at $z > 3$, where several DLAs exhibit $T_s > 2000$ K. Because the kinetic temperature, T, equals the spin temperature in most scenarios, the high values of T_s have been interpreted as indicators of gas in the WNM rather than CNM phase (Carilli et al. 1996; Kanekar & Chengalur 2001; Chengalur & Kanekar 2000). This poses an interesting dilemma, as C II* absorption, which must arise in the CNM in most DLAs, is detected in two DLAs with high inferred spin temperatures.

How do we reconcile the spin temperature limit, $T_s > 4000$ K (Ellison et al. 2001; Kanekar & Chengalur

2001), with the ≈ 100 K temperature predicted for the CNM in the $z = 3.387$ DLA toward Q0201+11? To answer this question, we consider the sizes of the CNM clouds relative to the background radio source in Q0201+11. Following the discussion in § 5.2, we find that the linear dimensions of CNM clouds are less than 10 pc, since $n_{CNM} \approx 6$ cm^{-3} and we have assumed half the total H I column density of 1.8×10^{21} cm^{-2} to be CNM gas equally distributed among five or more velocity components. To estimate the linear dimension subtended by the radio source at the DLA, we note that VLBI observations at $\nu = 1.6$ GHz show Q0201+11 to subtend a solid angle less than $\omega_{1.6} = 2.5 \times 5.0$ mas^2 (Hodges, Mutel, & Philips 1984). The solid angle of the source must be larger than $\omega_{1.6}$ at $\nu = 323.7$ MHz, the frequency of redshifted 21 cm absorption; otherwise, the brightness temperature of this radiation in the rest frame of the $z = 3.61$ QSO is $T_b(1492 \text{ MHz}) = 1.7 \times 10^{12}$ K. This exceeds the 10^{12} K Compton limit restricting the brightness temperature of sources such as Q0201+11, which belongs to the class of peak spectrum objects *not* exhibiting relativistic beaming (Phillips & Mutel 1982). To be consistent with the Compton limit, the source must subtend an effective linear diameter *exceeding* 40 pc at the DLA (where we assume $\Omega_M = 0.3$, $\Omega_\Lambda = 0.7$, and $h = 0.7$). As a result, the typical CNM cloud in this DLA covers a small fraction of the background radio source. This contrasts with the conclusions of de Bruyn, O'Dea, & Baum (1996), who did not consider the Compton limit.

It is now possible to understand the discrepancy between T_s and the temperature of the CNM. In the optically thin limit the apparent 21 cm optical depth $\tau(21) = f_{CNM}\tau_{CNM}(21)$, where f_{CNM} is the area covering factor of CNM gas, $\tau_{CNM}(21)$ is the 21 cm optical depth of a CNM cloud, $\tau(21) \equiv \ln(S_c/S_v)$, and S_v and S_c are the 373.3 MHz flux densities at Doppler velocity v and in the continuum, respectively. Chengalur & Kanekar (2000) placed a $1\,\sigma$ upper limit of 0.011 on $\tau(21)$. We shall be more conservative and assume a 95% confidence upper limit of $\tau(21) < 0.022$, which reduces the lower limit on T_s to 2000 K. Because half the sample DLAs show positive evidence for C II* absorption, while in three out of 25 DLAs there is probable evidence for WNM gas (see eq. [15] in Paper I), we find $0.5 < f_{CNM} < 0.88$. We shall assume $f_{CNM} = 0.67$ as this is in accord with the observed relative occurrence of multiple C II* velocity components in DLAs. As a result, we find $\tau_{CNM}(21) < 0.033$. To compute $N_{CNM}(\text{H I})$, the H I column density of the CNM cloud, we must estimate σ, the Gaussian velocity dispersion of the gas, since $N_{CNM}(\text{H I}) = 1.82 \times 10^{18}\tau_{CNM}(21)T_{CNM}\sqrt{2\pi}\sigma$. Assuming $\sigma = 9$ km s^{-1}, the velocity dispersion corresponding to the velocity width to which the upper limits on $\tau(21)$ apply, and $T_{CNM} \approx 100$ K, we find $N_{CNM}(\text{H I}) < 1.4 \times 10^{20}$ cm^{-2}. This is consistent with a total CNM H I column toward the optical continuum of 9×10^{20} cm^{-2} distributed among five or more components. In other words, the *inferred* spin temperature for the DLA toward Q0201+11 is high not because the temperature of the absorbing gas is high, but rather because the H I column densities of the foreground CNM clouds are low. In fact, there is evidence for a decrease in $N(\text{H I})$ with increasing redshift. Peroux et al. (2001) find the mean H I column density of DLAs is $\langle N(\text{H I}) \rangle = 3.9 \times 10^{20}$ cm^{-2} at $z > 3.5$, while $\langle N(\text{H I}) \rangle = 8.2 \times 10^{20}$ cm^{-2} at $z = 2.4$–3.5. Because these correspond to the total $N(\text{H I})$ rather than the CNM portion of the gas, it is plausible to

assume the mean H I column densities of CNM gas to be 2×10^{20} cm^{-2} at the DLA redshift $z = 3.38$. Therefore, it is not improbable for $N(\text{H I})_{CNM}$ to equal $(1$–$2) \times 10^{20}$ cm^{-2} in this DLA. If this interpretation is correct, the high H I column density $[N(\text{H I}) = 1.8 \times 10^{21}$ cm$^{-2}]$ and C II* detected in absorption toward Q0201+11 indicate that a larger than average number of CNM clouds are lined up toward the *optical* continuum source of this QSO. This is supported by the excessive number of low-ion clouds spread across a velocity interval of ~ 270 km s^{-1} (Ellison et al. 2001); by comparison, the median velocity interval of DLAs is ≈ 100 km s^{-1} (PW97). Note that Chengalur & Kanekar (2000) would not have detected this configuration, since it would have an apparent optical depth $\tau(21) = (10 \text{ pc}/40 \text{ pc})^2 5\tau_{CNM}(21) < 0.01$, which is less than the $2\,\sigma$ upper limit of 0.022.

Ellison et al. (2001) carried out an imaging study of the field surrounding Q0201+11 that provides a test of the CNM hypothesis. If C II* absorption in this DLA arises in WNM gas, the FUV intensities (at $\lambda = 1500$ Å), J_ν, would be higher than indicated by our CNM model. We find $(J_\nu)_{WNM} = 3.8 \times 10^{-18}$ ergs cm^{-2} s^{-1} Hz^{-1} sr^{-1}, while $(J_\nu)_{CNM} = 4.3 \times 10^{-19}$ ergs cm^{-2} s^{-1} Hz^{-1} sr^{-1} for the case of "Gal" dust and maximal depletion. Based on photometric redshifts, the leading candidate for the galaxy responsible for DLA absorption is object G2, the high surface brightness region of an $R \approx 25.3$ galaxy separated by $\Delta\theta = 2''.9$ from the QSO. If the FUV radiation emitted by G2 heats WNM gas responsible for C II* absorption, according to the bulge hypothesis G2 would be detected in the R band with flux density $S_{\nu_0} = 4\pi J_\nu(\Delta\theta)^2/(1 + z_{DLA})^3$, where $\nu = (1 + z_{DLA})\nu_0$. In this case the predicted AB magnitude is $R = 21.3$. If instead this WNM gas is heated by a uniform disk of sources centered on G2 and extending across the QSO sight line, the surface brightness of the disk would be $\mu_R = 26.4$ mag arcsec^{-2}. Both WNM scenarios are ruled out by the Ellison et al. (2001) images. In the bulge scenario G2 would be 4 mag brighter than observed, while in the uniform disk scenario the surface brightness of the disk would be detectable at the $4\,\sigma$ level in regions on the side of G2 away from the QSO. On the other hand, if G2 heats CNM gas responsible for C II* absorption, then $R = 23.6$ in the bulge scenario, while $\mu_R = 28.7$ mag arcsec^{-2} in the uniform disk scenario. Because of the large uncertainties in the R magnitude of G2, the bulge scenario is only marginally consistent with the data, while the uniform disk scenario is definitely consistent with the data. Therefore, the gas producing C II* absorption must be a CNM if it is heated by FUV radiation emitted by sources associated with G2. Of course, G2 may be incorrectly identified and the galaxy associated with the DLA could be located within the point-spread function of the QSO (Ellison et al. 2001), in which case C II* absorption could arise in either phase. This emphasizes the importance of obtaining a spectroscopic redshift for G2.

More recently, Kanekar & Chengalur (2003) deduced a 95% confidence lower limit of $T_s > 1.4 \times 10^4$ K for the $z = 3.062$ DLA toward Q0336−01. By contrast, we infer an equilibrium temperature of ≈ 100 K from the presence of C II* absorption in this DLA (see Table 1 in Paper I). In principle, we can explain the high inferred value of T_s with low values of $N(\text{H I})_{CNM}$ in this object also. However, much lower CNM filling factors are required as a result of the higher value of T_s. We think that it is more likely that the

high T_s inferred for this DLA is a by-product of a complex radio source structure. Although this source is observed to be compact at 5 GHz, it is likely to be extended at the much lower frequency predicted for redshifted 21 cm absorption. In fact, it is possible that the radio emission is concentrated in two equally bright components, each of which is symmetrically displaced more than 20 pc from the optical continuum (see Phillips & Mutel 1982). In that case the gas detected in optical absorption need not intercept radio frequency radiation along the line of sight. In any case it is difficult to understand how the lower limit on T_s can correspond to the temperature of neutral gas in any DLA, since 50% of H is collisionally ionized at 1.5×10^4 K.

6. SUMMARY AND CONCLUDING REMARKS

This paper expands on a new technique for measuring SFRs in DLAs developed in Paper I, namely, in Paper I we showed how detections of C II* $\lambda1335.7$ absorption could be used to infer the SFR per unit physical area, $\dot{\psi}_*$, in DLAs. We showed that a two-phase neutral medium, in which CNM gas is in pressure equilibrium with a WNM gas, is a natural by-product of thermal equilibrium. We also found that C II* absorption lines detected in DLAs could arise in either phase, but that significantly higher values of $\dot{\psi}_*$ were required if this absorption arose in the WNM. In this paper we use cosmological constraints to show that while the line of sight likely encounters both phases, C II* absorption arises mainly in the CNM. Our specific conclusions are as follows:

1. We compute the SFR per unit comoving volume in DLAs, $\dot{\rho}_*(z)$, by combining the mean SFR per unit area, $\langle\dot{\psi}_*(z)\rangle$, with the observed number of DLAs per unit absorption distance. We obtain statistically significant results for two redshift bins centered at $z = 2.15$ and 3.70; these are the first quantitative measurements of $\dot{\rho}_*$ at $z \approx 2$. The results show (1) $\dot{\rho}_*(z)$ for the WNM model is at least 10 times higher than for the CNM model, (2) $\dot{\rho}_*(z)$ for the CNM model is in approximate agreement with independent determinations from luminosities measured for flux-limited samples of galaxies, and (3) no evidence for evolution in the redshift interval $z = [1.6, 4.5]$. We also compute the bolometric background intensities, I_{EBL}, generated by the SFR histories, $\dot{\rho}_*(z)$. In every case the WNM models predict I_{EBL} above the observed 95% confidence upper limits. By contrast, the I_{EBL} predicted for the CNM models are consistent with this limit. As a result, models in which C II* absorption arises in WNM gas are ruled out. Finally, we develop a " consensus " model that accounts for the systematic errors arising from various model uncertainties. We also find that $\langle\dot{\psi}_*(z)\rangle$ for DLAs appears to decrease significantly with decreasing redshift at $z < 1.6$ if DLAs evolve into ordinary galaxies. To compute $\langle\dot{\psi}_*(z)\rangle$, we average $\dot{\psi}_*$ over $R_{H I}$ rather than the de Vaucouleurs radius.

2. We consider several consequences of our work. First, we evaluate the mass of stars and metals produced by the star formation histories we derived. Although the mass in stars produced by $z = 0$ is consistent with the masses of current stellar populations in current galaxies, the mass of metals produced by $z = 2.5$ is significantly higher than is observed for DLAs at that redshift. Various solutions to this dilemma come to mind, including ejection of metal-enriched

gas from DLA, making DLAs a transitory phase of galaxy evolution. However, this results in an IGM metallicity, $[M/H] = -1.2$, which is a factor of 100 larger than observed in the Lyα forest. Rather, we favor a scenario in which star formation and metal production occur in a centrally located bulge region displaced from the DLA gas. Second, we evaluate the bulge hypothesis and find that to within 10% accuracy the predicted $\dot{\rho}_*(z)$ agrees with that predicted by the uniform disk model used to derive the results discussed above. From the empirical upper limit on I_{EBL}, we find that the fraction of FUV radiation attenuated by optically thick dust in the bulge cannot exceed 0.7. Third, we search for evidence of connections between stars and gas. We find no evidence for a Kennicutt (1998) correlation between $\dot{\psi}_*$ and $N(H I)$. This is naturally explained by the bulge hypothesis in which SFRs in the bulge region are unrelated to the H I column density in regions giving rise to DLA absorption. The lack of a Kennicutt relation is also consistent with the model in which star formation occurs in the same region creating DLA absorption. This is because $\dot{\psi}_*$ is the SFR averaged over the entire DLA (5 kpc or more in most models), while $N(H I)$ is sampled over a transverse dimension corresponding to the linear diameter of the QSO, i.e., ~1 pc. On the other hand, when these quantities are averaged over the DLA sample, they are consistent with the Kennicutt relation, indicating that it may be present in a statistical sense. We also look for correlations between $\dot{\psi}_*$ and metallicity and between $\dot{\psi}_*$ and kinematic velocity width. Marginal evidence for correlations was found in the cases of metallicity and low-ion velocity width. Confirmation would indicate that both low-ion line width and metallicity are global parameters, which are determined by quantities such as dark matter mass. The reasons for null correlation in the case of $\dot{\psi}_*$ and high-ion velocity width are the same as for the Kennicutt relation.

3. We discussed tests of the ideas presented here. First, we present statistically significant evidence for a correlation between l_c and κ. This is consistent with grain photoelectric heating of CNM gas in DLAs with a limited range of SFRs, since $l_c \propto \kappa\epsilon\dot{\psi}_*$. We show that this correlation is not naturally explained by alternative heating mechanisms such as cosmic-ray ionization and X-ray photoionization. Second, we consider the possibility that the $^2P_{3/2}$ and $^2P_{1/2}$ fine-structure states in C^+ are populated by CMB radiation rather than collisions. In that case l_c would not equal the cooling rate, as we have assumed, but would instead reflect the local temperature of the CMB. We test this hypothesis by comparing the observed l_c with $(l_c)_{CMB}$, the spontaneous energy emission rate per H atom when CMB radiation alone populates the fine-structure states. We conclude that the CMB alone cannot explain the observed level of C II* excitation in 28 out of 30 DLAs. This is because the observed l_c do not show the sharp increase with redshift predicted for $(l_c)_{CMB}$ and because in all 28 cases $l_c \gg (l_c)_{CMB}$. The two exceptions are DLAs with upper limits on l_c and in which $(l_c)_{CMB} > 0.8l_c$. The implied cooling rates are very low and may indicate passage of the QSO sight lines through a WNM subjected to SFRs less than or equal to the mean $\langle\dot{\psi}_*\rangle$ deduced for most of our sample. In the third test, we use the ratio of C II* to resonance-line optical depths, $\mathscr{R}(v) = \tau_v(C II^*)/\tau_v(Si II)$, to probe the multiphase structure of the gas. Specifically, $\mathscr{R}(v)$ in the WNM should be $(l_c)_{WNM}/(l_c)_{CNM}$ times $\mathscr{R}(v)$ in the CNM. Because $(l_c)_{WNM}/(l_c)_{CNM} \approx 0.08$, $\mathscr{R}(v)$ should decrease significantly

at velocities corresponding to the WNM. Such variations may have been detected in one DLA. We also show how the WNM is easy to hide, and we discuss possible evidence for an increase in $\mathcal{R}(v)$ at velocities where $\dot{\psi}_*$ in the CNM increases.

4. We discuss possible objections to our picture of DLAs. The most persistent of these is the proposal that DLAs do not contain CNM gas but rather are comprised only of WNM gas. The first argument against the CNM is related to the large C II/C I ratios detected in DLAs, since this ratio is predicted to be lower in the CNM of the Milky Way ISM. However, this conclusion is sensitive to the ratio of X-ray and cosmic-ray heating rates to the SFR per unit area. In our models the X-ray heating rate is considerably lower than in the ISM. For our model parameters we are able to construct reasonable models predicting C II/C I ratios consistent with observations. The next argument against the CNM is that the hydrostatic pressures available in low-mass galaxy progenitors predicted for CDM theories are significantly lower than the values of P_{min} predicted for two-phase models. In that case, CDM models cannot generate sufficient pressure to create a two-phase medium. We show that this model is incorrect because the high values of P_{min} were based on an underestimate of the DLA metallicities at large redshifts. The third argument against the CNM stems from the high spin temperatures deduced from the low 21 cm optical depth, $\tau(21) < 0.02$, and high $N(\text{H I})$ $(=2 \times 10^{21}$ cm$^{-2})$ of a high-redshift DLA. How does one reconcile the large inferred spin temperature $(T_s > 2000 \text{ K})$ with the low temperatures $(T \sim 100 \text{ K})$ indicated by the detection of C II* absorption in this DLA? This answer is related to the geometry and H I column densities, $N(\text{H I})_{CNM}$, of the CNM clouds. Specifically, our models predict CNM clouds with sizes less than 10 pc, which is smaller than the diameter of the background radio source. In that case we find $N(\text{H I})_{CNM} \sim 10^{20}$ cm^{-2} for typical CNM clouds covering the high-z background radio source. Therefore, the inferred spin temperature is high not because the temperature of the absorbing gas is high, but rather because $N(\text{H I})_{CNM}$ is low. As a result, the large value of $N(\text{H I})$ toward the optical continuum source implies a larger than average number of CNM clouds along this line of sight, which is observed.

While we have attempted to evaluate important sources of systematic error, uncertainties still remain in our analysis. For example, we cannot rule out the possibility that the grain size distribution is radically different from the MRN model used in our calculations. However, we think that this is unlikely, as the MRN distribution nicely describes grain properties in local group galaxies that are linked to high-z DLAs by a similarity in the comoving density of stars in the galaxies to the comoving density of neutral gas in the DLAs. While the composition of the dust is also uncertain, sensitive searches for the $\lambda 2175$ feature will greatly reduce this source of systematic error. Second, although we have presented evidence for a two-phase medium in our DLA sample, in particular describing evidence for the presence of a WNM in three DLAs, the thermal state of the gas may differ from the equilibria envisaged in the models. Heiles (2001) has argued that warm clouds in the ISM have temperatures of ≈ 2000 K rather than the 8000 K predicted for the WNM. However, the C II* absorption we observe is unlikely to arise in such gas because at $T > 1000$ K the ratio of l_c to the total cooling (i.e., heating) rates is only slightly larger than predicted for the WNM. As a result, SFRs similar to those predicted for the WNM would be required and would likely exceed the observed upper limits on the bolometric background radiation intensity. There may be other caveats we have not discussed, but they are not obvious to us at this time.

Finally, we discuss the similarity between $\dot{\rho}_*(z)$ for DLAs and LBGs. Does it mean that they are the same objects? Schaye (2001) suggested that they were and that DLAs were created by the intersection between the line of sight to the QSO and gas outflow from foreground LBGs. He argued that since LBGs brighter than $R = 27$ have comoving densities $n_{co} = 0.016$ h^3 Mpc^{-3}, they could account for the incidence of DLAs provided that their H I cross-sectional radius is $r = 19$ h^{-1} kpc for a cosmology with $(\Omega_M, \Omega_\Lambda) = (0.3, 0.7)$. With our measurement of $\dot{\rho}_*$ we can compute the SFR per DLA, $\dot{M}_*$, because $\dot{\rho}_* = \dot{M}_* n_{co}$. From Table 1 we find $\dot{M}_* = 40$ $M_\odot$ yr^{-1} for $h = 0.7$. SFRs this high are ruled out by results from Hα imaging surveys of DLAs (Bunker et al. 2001; Kulkarni et al. 2001). Furthermore, in a recent search for a cross-correlation between DLAs and LBGs, Adelberger et al. (2003) found no evidence for an excess of LBGs with $R < 25$ near DLAs. As a result, current evidence suggests that DLAs and LBGs brighter than $R = 27$ are drawn from separate parent populations. However, more evidence is needed before this can be accepted as a robust result. If this is confirmed, the similarity between the SFRs per unit comoving volume of LBGs and DLAs would be a coincidence.

REFERENCES

Adelberger, K. L., Steidel, C. C., Shapley, A. E., & Pettini, M. 2003, ApJ, 584, 45
Bahcall, J. N., & Peebles, P. J. E. 1969, ApJ, 156, L7
Bakes, E. L. O., & Tielens, A. G. G. M. 1994, ApJ, 427, 822
Barger, A. J., Cowie, L. L., & Richards, E. A. 2000, AJ, 119, 2092
Bennett, C., et al. (WMAP Team). 2003, preprint (astro-ph/0302208)
Briggs, F. H., & Wolfe, A. M. 1983, ApJ, 268, 76
Bruzual, A., & Charlot, S. 1993, ApJ, 405, 538
Bunker, A. J., Warren, S. J., Clements, D. J., Williger, G. M., & Hewett, P. C. 1999, MNRAS, 309, 875
Carilli, C. L., Lane, W., de Bruyn, A. G., Braun, R., & Miley G. K. 1996, AJ, 111, 1830
Chengalur, J. N., & Kanekar, N. 2000, MNRAS, 318, 303
Cowie, L. L., Songaila, A., & York, D. G. 1979, ApJ, 230, 469
de Bruyn, A. G., O'Dea, C. P., & Baum, S. A. 1996, A&A, 305, 450
Dessauges-Zavadsky, M., D'Odorico, S., McMahon, R. G., Molaro, P., Ledoux, C., Peroux, C., & Storrie-Lombardi, L. J. 2001, A&A, 370, 426
Dickey, J. M., & Lockman, F. J. 1990, ARA&A, 28, 215
Dopita, M. A., & Ryder, S. D. 1994, ApJ, 430, 163
Draine, B. T. 1978, ApJS, 36, 595

Ellison, S. L., Pettini, M., Steidel, C. C., & Shapley, A. E. 2001, ApJ, 549, 770
Fukugita, M., Hogan, C., & Peebles, P. J. E. 1998, ApJ, 503, 518
Garnett, D. R., Shields, G. A., Skillman, E. D., Sagan, S. P., & Dufour, R. J. 1997, ApJ, 489, 63
Ge, J., & Bechtold, J. 1997, ApJ, 477, L73
Haehnelt, M. G., Steinmetz, M., & Rauch, M. 1998, ApJ, 495, 647
Hauser, M. G., & Dwek, E. 2001, ARA&A, 39, 249
Heiles, C. 2001, ApJ, 551, L105
Hodges, M. W., Mutel, R. L., & Philips, R. B. 1984, AJ, 89, 1327
Holland, W. S., et al. 1999, MNRAS, 303, 659
Kanekar, N., & Chengalur, J. N. 2001, A&A, 369, 42
———. 2003, A&A, 399, 857
Kennicutt, R. C., Jr. 1998, ARA&A, 36, 189
Kulkarni, S. R., & Heiles, C. 1987, in Interstellar Processes, ed. D. J. Hollenbach & H. A. Thronson (Dordrecht: Reidel), 87
Kulkarni, V. P., Hill, H. M., Schneider, G., Weymann, R. J., Storrie-Lombardi, L. J., Rieke, M. J., & Thompson, R. I. 2001, ApJ, 551, 37
Lane, W. M., Briggs, F. H., & Smette, A. 2000, ApJ, 532, 146
Lanzetta, K. M., Noriaki, Y., Pascarelle, S., Chen, H.-W., & Fernandez-Soto, A. 2002, ApJ, 570, 492
Ledoux, C., Srianand, R., & Petitjean, P. 2002, A&A, 392, 781
Leitherer, C. 1998, in Dwarf Galaxies and Cosmology, ed. T. X. Thuan, C. Balkowski, V. Cavatte, & T. T. Van (Paris: Editions Frontières), 42
Levshakov, S. A., Dessauges-Zavadsky, D'Odorico, S., & Molaro, P. 2002, ApJ, 565, 696
Lilly, S., Le Fevre, O., Hammer, F., & Crampton, D. 1996, ApJ, 460, L1
Liszt, H. 2002, A&A, 389, 393
Mac Low, M.-M., & Ferrara, A. 1999, ApJ, 513, 142
Madau, P., Ferguson, H. C., Dickinson, M. E., Giavalisco, M., Steidel, C. C., & Fruchter, A. 1996, MNRAS, 283, 1388
Madau, P., & Pozzetti, L. 2000, MNRAS, 312, L9
Mo, H. J., Mao, S., & White, S. D. M. 1998, MNRAS, 295, 319
Molaro, P., Levshakov, S. A., Dessauges-Zavadsky, M., & D'Odorico, S. 2002, A&A, 381, L64
Morrison, R., & McCammon, D. 1983, ApJ, 270, 119
Norman, A., & Spaans, M. 1997, ApJ, 480, 145
Padmanabhan, T. 1993, Structure Formation in the Universe (Cambridge: Cambridge Univ. Press)
Pei, Y. C., Fall, S. M., & Hauser, M. G. 1999, ApJ, 522, 604
Peroux, C., McMahon, R. M., Storrie-Lombardi, L. J., & Irwin, M. J. 2001, preprint (astro-ph/0107045)

Petitjean, P., Srianand, L., & Ledoux, C. 2002, MNRAS, 332, 383
Pettini, M. 1999, in Chemical Evolution from Zero to High Redshift, ed. J. R. Walsh & M. R. Rosa (Berlin: Springer), 233
Pettini, M., Smith, L. J., Hunstead, R. W., & King, D. L. 1994, ApJ, 426, 79
Phillips, R. B., & Mutel, R. L. 1982, A&A, 106, 21
Prochaska, J. X. 2003, ApJ, 582, 49
Prochaska, J. X., & Wolfe, A. M. 1997, ApJ, 487, 73 (PW97)
———. 2002, ApJ, 566, 68 (PW02)
Rosenberg, J. L., & Schneider, S. E. 2003, ApJ, 585, 256
Sarazin, C. L., Rybicki, G. B., & Flannery, B. P. 1979, ApJ, 230, 456
Savage, B. D., Meade, M. R., & Sembach, K. R. 2001, ApJS, 136, 631
Schaye, J. 2001, ApJ, 559, L1
Silva, A. I., & Viegas, S. M. 2002, MNRAS, 329, 135
Songaila, A. 2001, ApJ, 561, L153
Srianand, R., Petitjean, P., & Ledoux, C. 2000, Nature, 408, 931
Steidel, C. C., Adelberger, K. L., Giavalisco, M., Dickinson, M., & Pettini, M. 1999, ApJ, 519, 1
Storrie-Lombardi, L. J., & Wolfe, A. M. 2000, ApJ, 543, 552
Toomre, A. 1964, ApJ, 139, 1217
Turnshek, D. A., Rao, S. M., & Nestor, D. B. 2002, in ASP Conf. Ser. 254, Extragalactic Gas at Low Redshift, ed. J. Mulcahey & J. Stocke (San Francisco: ASP), 42
Vazquez-Semadeni, E., Gazol, A., & Scalo, J. 2000, ApJ, 540, 271
Walborn, N. R., et al. 1998, ApJ, 492, L169
Weingartner, J. C., & Draine, B. T. 2001, ApJS, 134, 263
Wolfe, A. M. 1995, in ESO Workshop on QSO Absorption Lines, ed. G. Meylan (Berlin: Springer), 13
Wolfe, A. M., & Prochaska, J. X. 1998, ApJ, 494, L15
Wolfe, A. M., Prochaska, J. X., & Gawiser, E. 2003, ApJ, 593, 215 (Paper I)
Wolfe, A. M., Turnshek, D. A., Smith, H. E., & Cohen, R. D. 1986, ApJS, 61, 249
Wolfire, M. G., Hollenbach, D., McKee, C. F., Tielens, A. G. G. M., & Bakes, E. L. O. 1995, ApJ, 443, 152 (W95)
Wolfire, M. G., McKee, C. F., Hollenbach, D., & Tielens, A. G. G. M. 2003, ApJ, 587, 287
Wyse, R. F. G., Gilmore, G., & Franx, M. 1997, ARA&A, 35, 637
Zwaan, M., Briggs, F. H., & Verheijen, M. 2002, in ASP Conf. Ser. 254, Extragalactic Gas at Low Redshift, ed. J. Mulcahey & J. Stocke (San Fransisco: ASP), 169